# Longitudinal and Transverse Elastic Waves in 1D Granular Materials Modeled as Micromorphic Continua

Anil Misra<sup>1\*</sup> and Nima Nejadsadeghi<sup>2</sup>

<sup>1</sup>Civil, Environmental and Architectural Engineering Department, <sup>2</sup>Mechanical Engineering Department,

University of Kansas, 1530 W. 15th Street, Learned Hall, Lawrence, KS 66045-7609. \*corresponding author: Ph: (785) 864-1750, Fax: (785) 864-5631, Email: amisra@ku.edu

For possible publication in:

Wave Motion

#### Abstract

In this paper, the granular micromechanics approach proposed by Misra and Poorsolhjouy (2016) is used to study the dispersive behavior of the granular materials in response to the elastic deformation waves. This study is motivated by the typical lack of connection between the mathematical models, the parameters involved, and the physics of granular material. Therefore, extensive parametric studies are done to understand how each intergranular stiffness coefficient contributes to the dispersive behavior of the material. Two cases of one dimensional wave propagation problems have been investigated. Case 1 focuses upon the longitudinal wave propagation in a one dimensional continuum, while case 2 considers the transverse wave propagation in a one dimensional continuum that has a two-dimensional micro-structure. Results predict the emergence of frequency band gaps and negative group velocities for certain values of the parameters involved. Such phenomena can be produced by starting from the micro-structure and producing a materials for which the inter-granular stiffness parameters are the ones the granular micromechanics approach predict. This, however, is not a one to one mapping, and therefore, sets of solutions to achieve a particular behavior might exist. The granular micromechanics, therefore, systematizes the design process and eliminates ad-hoc manners leading to large data libraries.

Keywords: micromorphic continuum; dispersion; micro-structure; frequency band gaps; metamaterials; granular micromechanics

## 1. Introduction

Many engineering and science disciplines such as material development, transportation and infrastructure systems [1, 2], pharmaceuticals, drug delivery, and natural processes in geophysics encompass the applications of granular materials, suggesting a necessity to better understand how such materials behave. Studying elastic wave propagation in granular media results in a better realization of how these materials react to external actions, and in general, promotes the understanding of such materials. Granular materials, due to their grain-scale mechanomorphological properties, have an inherent microstructural characteristic length with which the wavelength of excitation at high frequencies becomes comparable [3]. As a result, effects of the micro-mechano-morphology become significant when the material experiences high frequency loads. Therefore, it becomes important to include information about the material's micro-structure in wave propagation studies [4]. Notably, in these cases, the classical wave equation of the form of a hyperbolic partial differential equation becomes complicated as additional terms are introduced to account for the micro-mechano-morphology. A previous study on dielectric granular materials revealed the potential tenability of the range, and location of frequency bandgaps in the presence of external electric field using straightforward examples [5], but did not analyze thoroughly the material parameters' effects on the dispersive behavior of granular media. Such analysis is pursued in the present paper.

Herein, the granular micromechanics approach proposed in [6] to develop a micromorphic model is used to study the dispersive behavior of the granular materials in response to the elastic deformation waves. In granular micromechanics approach, the material representative volume element (RVE) is modeled as a collection of grains which are interacting with each other through different inter-granular mechanisms. This approach treats the problem in a statistical sense by considering mean behavior of grain-pairs [7]. The proposed approach to developing continuum models provides the framework to describe the average behavior of many types of granular materials. The approach taken is clearly different from that proposed in the literature by combining masses, linear springs, rotational springs, beams etc. (see for example [8-10]). Indeed, the ansatz to this approach can be traced to the work of Piola [11] and Hellinger [12]. Moreover, the necessity of extended continua including higher gradients of displacements as envisaged by Piola has been exemplified in the recent works of wave propagation [13-15].

In the continuum description based upon granular micromechanics approach, the material point is modeled as a granular volume element composed of distinct grains, and grain-pair interactions are elementary units of the material's microscopic behavior. The resulting continuum model is similar to the micro-structure elasticity model of [16] and micromorphic model of [17]. While there are works in the recent literature that consider wave propagation in micromorphic media [3, 4, 18, 19], typically, the considered physics has a weak relation to materials with granular micro-structure. To this extent, the current work is motivated by the lack of connection between the mathematical models, the parameters involved, and the physics of granular materials. Here we explore this connection through a theoretical approach, since the complexities of measuring parameters in experiments are typically unsurmountable and experimental approaches fail to provide a comprehensive analysis of the behavior of the materials with micro-structures. The paper is organized as follows.

An overview of the theory is presented in section 2, where the kinematics of the model and the variational approach to derive the governing equations of motion are introduced. To avoid complexities, and to be better able to interpret the role of the micro-structure in the dispersive behavior of the granular materials, we limit our studies to two cases of one dimensional wave propagation. We perform extensive parametric studies to emphasize the effect of micro- and macro-scale parameters on the dispersive behavior of the material. Case 1 focuses upon the longitudinal wave propagation in a one dimensional continuum with granular micro-structure which is described in section 3. Case 2 considers the transverse wave propagation in a one dimensional continuum that has a two-dimensional granular micro-structure as described in section 4. Section 5 is devoted to the micro-mechanical implication of the analyses presented in sections 3 and 4, where a connection between the observed behavior and the grain-pair interactions is made. Furthermore, a discussion on the potential applicability of the theory used here in the design and fabrication of granular metamaterials with specific material properties for particular purposes is made. Finally, the summary and conclusion of the present work is embraced in the section 6, where the possibility for future research is also proposed.

# 2. Micromorphic Model based upon Granular Micromechanics

The granular micromechanics proceeds from an identification of the grain-scale motions in terms of the continuum measures and the volume average of grain-pair interaction energies with the macro-scale deformation energy density. In the current format of granular micromechanics [20], two grain-scale kinematic measures are defined, one for determining relative displacements and the other for relative rotations. It is remarkable that the considered grain-scale kinematic measures represent the combined effect of the grain centroid displacement, spin and size, and do not follow the decomposition adopted in some previous attempts of micro-macro identifications [21-23]. These grain-scale motions are identified with six set of continuum kinematic measures that include the macro-scale displacement/rotation gradients, micro-scale displacement/rotations gradients identified with displacement/rotation fluctuations within a material point, and macro-gradient of the micro-scale displacement/rotation gradients. The deformation energy density of a material point is then expressed in terms of the kinematic measures at the two scales and the inter-granular force measures as well as the continuum stress are defined as conjugates of the kinematic measures. Subsequently, the relationships are derived between stress and inter-granular forces that include stretch/compression, tangential, bending and torsional actions as well as for further derivation of the constitutive relations, variational principle, and balance equations for non-classical micromorphic model whose parameters can be identified in terms of the grain-scale properties [6, 24, 25]. In what follows, we briefly state the mathematical model and derive the equations of motion. The reader is referred to [6, 20] for more detailed description.

To develop a continuum model, each material point is considered a representative volume element (RVE), as shown in Fig. 1. Consider the coordinate system x to be relevant to the global (macroscale) model, and attach a local or micro-scale coordinate system x' to the material point P or the barycenter of the RVE with its axes parallel to the global coordinate system axes x. The microscale coordinate system is defined such that it is able to distinguish different grains inside the material point. The displacement of the grains are then not only a function of the coordinates of the material point P, but also of the micro-scale coordinates of the grain within the material point, i.e.,

$$\phi_i = \phi_i(x, x', t), \tag{1}$$

where  $\phi_i$  is the displacement of grain centroids. Now consider the displacement,  $\phi_i^p$ , of the centroid of grain, p, contained within the continuum material point, where the displacement is defined in [6]. Utilizing the Taylor's expansion, this displacement can be related to the displacement,  $\phi_i^n$ , of the centroid of neighboring grain, n, such that the difference will be the relative displacement,  $\delta_i^{np}$ , of the two grains, which is given as follows, where we have included only the first and second order terms in the Taylor series expansion

$$\delta_i^{np} = \phi_i^p - \phi_i^n = \phi_{i,j}^n l_j + \frac{1}{2} \phi_{i,jk}^n l_j l_k.$$
 (2)

In Eq. (2),  $l_j$  is the vector joining the centroids of n and p, and the tensor product  $l_j l_k$  (= $J_{jk}$ ) is a geometry moment tensor. The differentiation in Eq. (2) is with respect to x'. In the rest of the paper, a comma in the subscript means derivation with respect to the position, and dots on the parameters express derivations with respect to time. Also note that the summation convention over repeated indices (in the subscript) is implied unless noted otherwise. Following a similar analysis, the relative rotations of two interacting grains, n and p, denoted by  $\theta_i$  is found as [6]

$$\theta_i^{np} = e_{iki} \phi_{k,ip} l_p \,, \tag{3}$$

where  $e_{ijk}$  is permutation symbol and the differentiation is with respect to x'. We introduce the decomposition of the displacement gradient field as [6, 20, 26]

$$\psi_{ij} = \phi_{i,j} = \overline{\phi}_{i,j} - \gamma_{ij} , \qquad (4)$$

where  $\psi_{ij}$  is the displacement gradient in the RVE,  $\overline{\phi}_{i,j}$  is the macro-scale displacement gradient which is a constant in a material point, and  $\gamma_{ij}$  is the relative deformation due to the fluctuations of the micro-displacement of the grains inside the RVE. This suggests that the micro-deformation  $\psi_{ji}$  is taken to be homogenous in the RVE but can be non-homogenous in the macro-medium. The relative displacement of grains p and n can then be decomposed as

$$\delta_i^{np} = \overline{\phi}_{i,j} l_j - \gamma_{ij} l_j + \frac{1}{2} \phi_{i,jk} l_j l_k = \delta_i^M - \delta_i^M + \delta_i^g,$$
(5)

where

$$\delta_i^M = \overline{\phi}_{i,j} l_j, \quad \delta_i^m = \gamma_{ij} l_j, \quad \delta_i^g = \frac{1}{2} \phi_{i,jk} l_j l_k. \tag{6}$$

With regards to Eq. (6),  $\delta_i^M$  is due to the average displacement gradient,  $\overline{\phi}_{i,j}$ ,  $\delta_i^M$  is due to the gradients of the fluctuation in grain displacement,  $\gamma_{ij}$ , and  $\delta_i^g$  is due to the second gradient term,  $\phi_{i,jk}$ , which is same as the gradient of the relative deformation,  $\gamma_{ij,k}$ .

Macro-scale deformation energy density W of the granular continua can be defined as a function of the continuum kinematic measures as

$$W = W\left(\overline{\phi}_{(i,j)}, \gamma_{ij}, \phi_{i,jk}\right),$$
(7)

where  $\overline{\phi}_{(i,j)}$  is the symmetric part of the macro-scale displacement gradient. Macro-scale stress components conjugate to these kinematic measures are obtained as

$$\tau_{ij} = \frac{\partial W}{\partial \overline{\phi}_{(i,j)}} = \frac{\partial W}{\partial \varepsilon_{ij}}, \quad \sigma_{ij} = \frac{\partial W}{\partial \gamma_{ij}}, \quad \mu_{ijk} = \frac{\partial W}{\partial \gamma_{ij,k}}, \tag{8}$$

where  $\tau_{ij}$ ,  $\sigma_{ij}$ , and  $\mu_{ijk}$  are Cauchy stress, relative stress, and double stress, respectively. Macroscale deformation energy density can be expressed in terms of micro-scale deformation defined for the  $\alpha^{th}$  interacting pair as  $W^{\alpha}\left(\delta_{i}^{\alpha M}, \delta_{i}^{\alpha m}, \delta_{i}^{\alpha g}, \theta_{i}^{\alpha u}\right)$ , such that

$$W = \frac{1}{V'} \sum_{\alpha} W^{\alpha} \left( \delta_i^{\alpha M}, \delta_i^{\alpha m}, \delta_i^{\alpha g}, \theta_i^{\alpha u} \right). \tag{9}$$

In Eq. (9) V' is the volume of the assumed RVE. The intergranular force and moment conjugates are introduced, using Eq. (9), as

$$\frac{\partial W}{\partial \delta_i^{\alpha \zeta}} = f_i^{\alpha \zeta}; \quad \zeta = M, m, g, \quad \frac{\partial W}{\partial \theta_i^{\alpha u}} = m_i^{\alpha u}. \tag{10}$$

Substituting Eq. (9) in Eq. (8), and using Eq. (6) and Eq. (10), it follows that [6]

$$\tau_{ij} = \frac{1}{V'} \sum_{\alpha} f_i^{\alpha M} l_j^{\alpha}, \quad \sigma_{ij} = \frac{1}{V'} \sum_{\alpha} f_i^{\alpha m} l_j^{\alpha}, \quad \mu_{ijk} = \frac{1}{V'} \left( \sum_{\alpha} f_i^{\alpha g} J_{jk}^{\alpha} + \sum_{\alpha} m_l^{\alpha u} e_{jil} l_k^{\alpha} \right). \tag{11}$$

Therefore, the macro-scale stress measures are defined in terms of the inter-granular forces, branch vector, and the geometry moment tensor.

Defining a local coordinate system for each interacting grain pair, decomposing intergranular force, moment, displacement, and rotation vectors in their normal and tangential components, and assuming a quadratic form of  $W^{\alpha}$  for linear isotropic elasticity case, the macro-scale constitutive relationships in the global coordinate system are derived [6] as

$$\tau_{ij} = C_{ijkl}^M \varepsilon_{kl}, \quad \sigma_{ij} = C_{ijkl}^m \gamma_{kl}, \quad \mu_{ijk} = \left( A_{ijklmn}^g + A_{ijklmn}^u \right) \phi_{l,mn}, \tag{12}$$

where  $C_{ijkl}^{M}$  and  $C_{ijkl}^{m}$  are fourth rank tensors, and  $A_{ijklmn}^{g}$  and  $A_{ijklmn}^{u}$  are sixth rank tensors, defined as (Refer to [6] for more details)

$$C_{ijkl}^{M} = \frac{1}{V'} \sum_{\alpha} K_{ik}^{M} l_{i}^{\alpha} l_{j}^{\alpha}, \quad C_{ijkl}^{m} = \frac{1}{V'} \sum_{\alpha} K_{ik}^{m} l_{i}^{\alpha} l_{j}^{\alpha},$$

$$A_{ijklmn}^{g} = \frac{1}{V'} \sum_{\alpha} K_{il}^{g} J_{mn}^{\alpha} J_{jk}^{\alpha}, \quad A_{ijklmn}^{u} = \frac{1}{V'} \sum_{\alpha} G_{pq}^{u} e_{mlq} e_{jip} l_{k}^{\alpha} l_{i}^{\alpha}.$$
(13)

We note here that for many granular systems (including those formed by grain-packings for which Hertz Law has been used widely [27]), grain-pair interactions are nonlinear and include dissipation. Nevertheless, understanding linear elastic behavior has practical significance for small amplitude vibrations, for which a quadratic form of  $W^a$  can be assumed. In addition, linear elastic behavior provides a point of departure for exploring more complex phenomena introduced by nonlinearity and dissipation. In Eq. (13), the four different inter-granular stiffness measures are defined as  $K_q^p$  and  $G_q^u$ , where K and G denote the stretch and rotational stiffnesses, respectively, p=M, m and g; q=n, w. Further in Eq. (13), superscript M denotes macro-stiffness, m denotes the micro-stiffness, m denotes the second gradient stiffness, and m denotes the rotation terms, respectively, introduced for each term of the decomposed relative displacement and rotation; and the subscripts m and m refer to the normal and tangential grain-pair interaction directions.

We now briefly outline the derivation of the balance equations and equations of motion for a material with granular micro-structure using a variational approach. To this end, we can write for the variation of the internal potential energy, using Eq. (4) and Eq. (8)

$$\delta W = \tau_{ij} \delta \varepsilon_{ij} + \sigma_{ij} \delta \gamma_{ij} + \mu_{ijk} \delta \phi_{i,jk} = \tau_{ij} \delta \overline{\phi}_{(i,j)} + \sigma_{ij} \left( \delta \overline{\phi}_{(i,j)} - \delta \phi_{i,j} \right) + \mu_{ijk} \delta \phi_{i,jk}. \tag{14}$$

Using Leibniz differentiation rule, we can write Eq. (14) in the form

$$\delta W = \left[ \left( \tau_{ij} + \sigma_{ij} \right) \delta \overline{\phi}_i \right]_i - \left( \tau_{ij} + \sigma_{ij} \right)_i \delta \overline{\phi}_i - \sigma_{ij} \delta \psi_{ij} + \left( \mu_{ijk} \delta \psi_{ij} \right)_k - \mu_{ijk,k} \delta \psi_{ij} . \tag{15}$$

The variational of the macro-scale deformation energy functional can be obtained using Gauss's divergence theorem of integration and Eq. (15) as

$$\delta \tilde{V} = \int_{V_{ij}} + \sigma_{ij} \int_{J_i} \delta \overline{\phi}_i dV - \int_{V_i} \left( \mu_{ijk,k} + \sigma_{ij} \right) \delta \psi_{ij} dV + \int_{S_i} \left( \tau_{ij} + \sigma_{ij} \right) n_j \delta \overline{\phi} dS + \int_{S_i} \mu_{ijk} n_k \delta \psi_{ij} dS .$$
 (16)

We also define the variational of the external work as

$$\delta \tilde{V} = \delta \bar{\phi_i} dV + \int_V \Phi_{ij} \delta \psi_{ij} dV + \int_S t_i \delta \bar{\phi} dS + \int_S T_{ij} \delta \psi_{ij} dS , \qquad (17)$$

where  $f_i$  is the non-contact volumic (body) force per unit volume,  $t_i$  is the contact traction defined as a surface force per unit area,  $\Phi_{ij}$  is the non-contact volumic (body) double force per unit volume, and  $T_{ij}$  is the contact double traction defined as double force per unit area.

The kinetic energy density (kinetic energy per unit macro-volume) T is defined as

$$T = \frac{1}{V'} \int_{V'} \frac{1}{2} \rho' \zeta \qquad , \tag{18}$$

where  $\rho'$  is the micro-scale mass density per unit macro-volume. For a constant  $\rho'$  in the RVE and the continuum, we have, for the macro-scale mass density per unit macro-volume,

$$\rho = \frac{1}{V'} \int_{V'} \rho' dV' = \frac{\rho'}{V'} \int_{V'} dV' = \rho'. \tag{19}$$

Therefore, the densities in micro- and macro-scales become identical. Note that for graded materials with spatially varying densities, one can take  $\rho'$  to be non-uniform. This assumption leads to additional terms in the final form of the kinetic energy derived in this paper, and will be pursued in future publications. Eq. (18), after substituting for  $\phi_i$ , using Eq. (19), and neglecting higher order inertia terms, can be written as

which is similar to [28], and where  $d_{jk}$  is defined as follows

$$d_{jk} = \frac{1}{V'} \int_{V'} x'_j x'_k dV' \,. \tag{21}$$

In the rest of the paper, we assume the RVE to be cubic with edges 2d parallel to the axes x'. In such a case, Eq. (21) simplifies to

$$d_{jk} = \frac{1}{3}d^2\delta_{jk}\,, (22)$$

where  $\delta_{jk}$  is the Kronecker delta. From Eq. (22) it is clear that  $d_{jk}$  is a diagonal matrix with equal diagonal terms. The total kinetic energy is the integral of the kinetic energy density over the whole domain, and is written as

$$\tilde{I}$$
 (23)

Using Eq. (20) and Eq. (23), the variational of the kinetic energy functional is written, after integration by parts and assuming the values of  $\overline{\phi}_j$  and  $\psi_{ij}$  to be known at  $t = t_0, t_1$ , as

$$\delta \int_{t_0}^{t_1} \tilde{1} \qquad \dot{t} = \int_{t_0}^{t_1} \int_{V} \frac{1}{3} \rho d^2 t \qquad \forall dt.$$
 (24)

Hamilton principle requires the action functional to be minimum, and is expressed as

$$\delta \int_{t_0}^{t_1} \left( \tilde{I} - \tilde{I} - \tilde{I} \right) dt = 0. \tag{25}$$

Substituting Eq. (16), Eq. (17), and Eq. (24) in Eq. (25) results in the balance equations and the boundary conditions. The balance equations are

$$(\tau_{ij} + \sigma_{ij})_{,j} + f_i = \rho_{i,j}$$

$$\mu_{ijk,k} + \sigma_{ij} + \Phi_{ij} = \frac{1}{3}\rho d^2 \iota^{\prime\prime}$$
(26)

and the two natural boundary conditions given in terms of the stress measures are

$$\left(\tau_{ii} + \sigma_{ii}\right)n_i = t_i, \quad \mu_{iik}n_k = T_{ii}. \tag{27}$$

Finally, equations of motion can be derived, by substituting the constitutive equations, Eq. (12), in the balance equations, Eq. (26). Assuming volumic (body) forces and volumic double forces to be absent, the equations of motion are described as

$$\left(C_{ijkl}^{M} + C_{ijkl}^{m}\right)\overline{\phi}_{k,lj} - C_{ijkl}^{m}\psi_{kl,j} = \rho$$

$$\left(A_{ijklmn}^{g} + A_{ijklmn}^{u}\right)\psi_{lm,nk} + C_{ijkl}^{m}\overline{\phi}_{k,l} - C_{ijkl}^{m}\psi_{kl} = \frac{1}{3}\rho d^{2}i$$
(28)

# 3. Longitudinal wave propagation in a 1D isotropic continuum with granular micro-structure

### 3.1. Mathematical Formulation

In what follows, we consider the longitudinal (P) wave propagation in an isotropic one dimensional infinite continuum in macro- and micro-scale along the  $x_1$  axis. A schematic of the general problem has been shown in Fig. 2. Note again that a 1D homogenous isotropic continuum can be, in general, non-homogenous in the RVE (micro-scale). This inhomogeneity may come from the mass density distribution, or the variation of grain pair interaction in the medium. The former is depicted in Fig. 2, while the latter is rather difficult to visualize. As the underlying assumption for deriving Eq. (31) is having a constant  $\rho'$ , our focus in this section is inhomogeneity in grain-pair interactions. In this case, the twelve equations of motion Eq. (28) reduce to the following two equations

$$(P+Q)\bar{\phi}_{1,11} - Q\psi_{11,1} = \rho_{1...}$$

$$R\psi_{11,11} + Q\bar{\phi}_{1,1} - Q\psi_{11} = I_1^{"}$$
(29)

where the symbols P, Q, R, and I have been used for brevity, to represent the macro-scale modulus  $C_{1111}^M$ , the micro-scale modulus  $C_{1111}^m$ , the second-gradient modulus  $A_{111111}^g$ , and micro-inertia  $\frac{1}{3}\rho d^2$ , respectively. Solutions of the Eq. (29) are of the form

$$\bar{\phi}_1 = \bar{\phi}_1(x_1, t), \quad \psi_{11} = \psi_{11}(x_1, t),$$
(30)

in which the kinematic measures  $\overline{\phi}_1$  and  $\psi_{11}$  are only functions of time and  $x_1$ . Following Mindlin [16] and specializing the solutions in Eq. (30) to harmonic plane waves, we will have the following form for the solution of Eq. (29)

$$\overline{\phi_{l}} = \operatorname{Re}\left(A_{l}i\,e^{i(kx_{l}-\omega t)}\right), \quad \psi_{11} = \operatorname{Re}\left(B_{11}\,e^{i(kx_{l}-\omega t)}\right),\tag{31}$$

where k is the wave number,  $\omega$  is the angular frequency (to which we refer for the rest of the paper as frequency),  $A_1i$  and  $B_{11}$  are the amplitudes of the macro displacement and micro displacement gradient, respectively, and  $i^2 = -1$ . Note that the amplitudes Ai and B can take complex values.

Substituting Eq. (31) into Eq. (29), the set of equations can be rewritten in the following matrix form

$$\begin{bmatrix} c_0^2 k^2 & c_A^2 k \\ \frac{k}{p^2} & \frac{p^2 c_1^2 k^2 + 1}{p^2} \end{bmatrix} \begin{bmatrix} A_1 \\ B_{11} \end{bmatrix} = \omega^2 \begin{bmatrix} A_1 \\ B_{11} \end{bmatrix}, \tag{32}$$

where, following [4], we have introduced the velocities,  $c_0$ ,  $c_1$ , and  $c_A$ , and characteristic time, p as follows

$$c_0^2 = \frac{P+Q}{\rho}, \quad c_1^2 = \frac{R}{I}, \quad c_A^2 = \frac{Q}{\rho}, \quad p^2 = \frac{I}{Q}.$$
 (33)

Eq. (32) is an eigenvalue problem with the eigenvalue  $\omega^2$  and the eigenvector comprising the amplitudes of the propagating macro-displacement waves and micro-displacement gradient waves, respectively. The relationship between the components  $A_1$  and  $B_{11}$  is given, using Eq. (32), as

$$B_{11} = A_1 \left( \frac{\omega^2 - c_0^2 k^2}{c_4^2 k} \right). \tag{34}$$

Solving for the eigenvalues  $\omega^2$ , Eq. (32) yields the secular equation

$$\omega^2 = (c_0^2 - c_A^2)k^2 + p^2(\omega^2 - c_0^2k^2)(\omega^2 - c_1^2k^2).$$
(35)

Eq. (35) is the dispersion relation for the problem under study. A similar form of dispersion relation

can be found, for example in [4, 29]. It is noteworthy that the parameters introduced in this paper can be identified with those in [4, 29] as follows:  $\hat{\alpha} = (P + Q)$ ,  $\hat{B} = -\hat{A} = Q$ ,  $\hat{C} = R$ . What is noteworthy in the present paper is the connection of these parameters with the micro-measures (such as micro-stiffnesses and grain sizes) relevant for elastic granular systems. This connection between the continuum models and micro-measures presents a new paradigm for exploring the micro-mechanical antecedents of phenomena predicted by Eq. (35), which are described in further in section 5. In very low frequency/wavenumber ranges, higher order terms of frequency and wave number in Eq. (35) can be neglected and the waves propagate, expectedly, with the macro-scale velocity  $\sqrt{c_0^2-c_A^2}$ , related only to the macro-scale moduli and density as  $\frac{P}{\rho}$ . Although it appears that the effect of micro-structure is seemingly lost in the first part of the right hand side of Eq. (35), however it is to be noted that the grain-scale effects are reflected in the macro-scale moduli and density (as seen from Eq. (13) and Eq. (19)). Furthermore, microstructural effects become increasingly prominent for larger frequencies and wavenumbers through the terms  $c_0$  and  $c_1$  in the second part of the right hand side of Eq. (35). Clearly, Eq. (35) shows that for very small frequencies and wavenumbers, fluctuation in grain-pair stiffnesses in the RVE has negligible effect and wave propagation is controlled by the macro-scale properties, while in larger frequencies and wavenumbers, the effect of fluctuation in grain-pair stiffnesses on the velocity of propagating waves become increasingly significant through the micro-moduli, second-gradient moduli and micro-inertia whose antecedents are further discussed in section 5.

Introducing the dimensionless wave number and frequency

$$\xi = pc_0 k, \quad \eta = p\omega, \tag{36}$$

and dimensionless velocities

$$\gamma_A = \frac{c_A}{c_0} = \sqrt{\frac{Q}{P + Q}}, \quad \gamma_1 = \frac{c_1}{c_0} = \sqrt{\frac{R}{P + Q}} \sqrt{\frac{\rho}{I}}.$$
(37)

Eq. (35) can be recast in the form

$$\eta^2 = (1 - \gamma_A^2) \xi^2 + (\eta^2 - \xi^2) (\eta^2 - \gamma_1^2 \xi^2). \tag{38}$$

We also introduce the parameter  $B'_{11}$  as

$$B_{11}' = pc_0 B_{11}. (39)$$

Now, using Eq. (34), Eq. (36), Eq. (37), and Eq. (39), we can write

$$B'_{11} = \frac{\eta^2 - \xi^2}{\gamma_A^2 \xi} A_1. \tag{40}$$

By introducing the dimensionless parameter  $\beta$  defined as the ratio of  $B'_{11}$  to  $A_1$ , we can rewrite Eq. (40) as

$$\beta = \frac{\eta^2 - \xi^2}{\gamma_4^2 \xi} \,. \tag{41}$$

The phase and group velocities can be obtained as follows

$$v_p = \frac{\omega}{k}, \quad v_g = \frac{d\omega}{dk},$$
 (42)

where  $v_p$  is the phase velocity, and  $v_g$  is the group velocity. Introducing the dimensionless phase and group velocities, respectively, as

$$\upsilon_p = \frac{v_p}{c_0}, \quad \upsilon_g = \frac{v_g}{c_0},$$
(43)

and using Eq. (36) and (42), we can write Eq. (43) in the form

$$\upsilon_p = \frac{\eta}{\xi}, \quad \upsilon_g = \frac{d\eta}{d\xi}.$$
(44)

Also, the mechanical energy transfer ratios associated with the micro-scale and macro-scale degrees of freedom can be obtained, using Eq. (31), Eq. (33), and Eq. (41) and considering the time average of the mechanical energy density over a time period as

$$\frac{E_{micro}}{E_{total}} = \frac{\frac{1}{2T} \int_{t}^{t+T} \left( I_{i} + R\psi_{11,1}^{2} \right) dt}{\frac{1}{2T} \int_{t}^{t+T} \left( I_{i} + R\psi_{11,1}^{2} + \rho_{i} \right) dt} + R\psi_{11,1}^{2} + \rho_{i} dt} \\
= \frac{\beta^{2} \left( \gamma_{A}^{2} \eta^{2} + \gamma_{A}^{2} + \gamma_{A}^{2} \gamma_{1}^{2} \xi^{2} \right)}{\beta^{2} \left( \gamma_{A}^{2} \eta^{2} + \gamma_{A}^{2} + \gamma_{A}^{2} \gamma_{1}^{2} \xi^{2} \right) + \eta^{2} + \xi^{2} - \gamma_{A}^{2} \xi^{2}}, \tag{45}$$

$$\frac{E_{macro}}{E_{total}} = 1 - \frac{E_{micro}}{E_{total}} = \frac{\eta^{2} + \xi^{2} - \gamma_{A}^{2} \xi^{2}}{\beta^{2} \left( \gamma_{A}^{2} \eta^{2} + \gamma_{A}^{2} + \gamma_{A}^{2} \gamma_{1}^{2} \xi^{2} \right) + \eta^{2} + \xi^{2} - \gamma_{A}^{2} \xi^{2}}.$$

## 3.2 Results

From the first of Eq. (37), it is clear that dimensionless velocity  $\gamma_A$  has lower bound limit of 0 and upper bound limit of 1. Very small values of  $\gamma_A$  represent materials in which the micro-stiffness is negligible compared to their macro-stiffness, and values close to the upper bound level have large micro-stiffness compared to their macro-stiffness. A value of  $\gamma_A = 0.71$  corresponds to approximately equal macro- and micro-stiffness of the material. On the other hand,  $\gamma_1$  has lower bound of 0 and an upper bound that can theoretically tend to infinity. For a particular ratio of macro-density to micro-inertia, larger  $\gamma_1$  implies a growing dominance of second gradient behavior. Fig. 3, Fig. 4, Fig. 5, and Fig. 6 show the dispersion curves, phase velocities, group velocities, and the energy transfer ratios of the micro-scale degree of freedom to the total energy transferred for different values of  $\gamma_A$  and  $\gamma_1$ . We observe in the case where second gradient terms are small (Fig. 3 and Fig. 5), increasing  $\gamma_A$  and decreasing  $\gamma_1$  leads to emergence of frequency

band gaps. For  $\gamma_1$  larger than a certain limiting value the stopband vanishes. The reason for the vanishing of band gaps can be understood by examining the group velocity plots in Fig 5. We note that the dimensionless group velocity of the optical and acoustic branches have the values of 0 and  $\sqrt{1-\gamma_A^2}$  (corresponding to group velocities of 0 and  $\sqrt{c_0^2-c_A^2}$  ) at small wavenumbers and asymptotic values of 1 and  $\gamma_1$  (corresponding to group velocities of  $c_0$  and  $c_1$ ), respectively. Therefore, a large value for the group velocity of the acoustic branch in both its small and large wavenumber ranges is the cause for vanishing band gaps. Complete band gaps emerge when the asymptote of the acoustic branch at large wavenumbers is a horizontal line. However, band gaps over a wide range of wavenumbers exist even for non-vanishing small values of  $\gamma_1$ . The starting point of the dimensionless frequency range in which the band gap appears varies, but is always between 0 and 1, while the end point of the dimensionless frequency is fixed at 1, corresponding to the frequency  $\omega = \sqrt{\frac{Q}{I}}$ , which is a function of the micro-scale properties. Also as  $\gamma_A$  increases and  $\gamma_1$  decreases, size of the band gap grows. Dimensionless phase velocity for the optical branch starts at infinity and reaches the value of 1 (phase velocity of  $c_0$ ) for large wavenumbers regardless of the value of  $\gamma_1$  (phase velocity of  $c_1$ ). The acoustic branch has an initial dimensionless phase velocity of  $\sqrt{1-\gamma_A^2}$  (phase velocity of  $\sqrt{c_0^2-c_A^2}$ ) and therefore, depends solely on the macro-scale stiffness of the material, while the asymptotic value reaches  $\gamma_1$  (phase velocity of  $c_1$ ). Therefore, based on the values of the parameters  $\gamma_A$  and  $\gamma_1$  we may have decreasing or increasing phase and group velocities of the acoustic branch depending on the values of  $\,\gamma_{\scriptscriptstyle A}\,$  and  $\,\gamma_{\scriptscriptstyle 1}\,$ .

In materials with very large second gradient properties ( $\gamma_1 > 1$ ), as seen in Fig. 4 and Fig. 6, the acoustic branch at small wavenumbers starts with the dimensionless phase and group velocities of  $\sqrt{1-\gamma_A^2}$  (corresponding to phase and group velocities  $\sqrt{c_0^2-c_A^2}$ ), which is similar to the previous case. However, in this case, the terms containing higher orders of  $\xi$  and  $\gamma_1$  in the dispersion relation become dominant as we evaluate their limit at high wavenumbers. Hence, the asymptotic slope of the dispersion curve for the optical branch becomes  $\gamma_1$  (corresponding to the asymptote  $\omega = c_1 k$ ), and that of the acoustic branch becomes 1 (the asymptote  $\omega = c_0 k$  with asymptotic phase

and group velocity of  $c_0$ ). This means for the cases where  $\gamma_1 > 1$ , the asymptotes of the two branches switch. Therefore, it is not possible to have stopbands.

We further observe that the energy transfer in 1D granular continuum during wave transmission occurs via two mechanisms, one governed by the macro-, and the other by the micro-scale degrees of freedom of the material. According to Fig. 3, in the acoustic branch at small wave numbers, energy transfer is affected mainly by the macro-scale degree of freedom, while for larger wave numbers, micro-scale degree of freedom plays the main part in energy transfer. This obviously shows the hierarchical nature of the wave propagation in micro-structured media. Large values of  $\gamma_1$  result in smoother shift from macro to micro-scale degree of freedom mechanism. In the case of optical wave, at small wavenumbers, the energy transfer is purely governed by the micro-scale degree of freedom. The model predicts transition of energy transfer mechanism from micro- to macro-scale, but it is well understood that for such large wavenumbers, the characteristic length of the excitation can be smaller than the characteristic length of the micro-structure, and hence, the proposed continuum mechanics theory may not be applicable. Note that when both  $\gamma_A$  and  $\gamma_1$  take very small values (e.g., in Fig. 3 for  $\gamma_A = 0.03$  and  $\gamma_1 = 0.0002$ ), we reach the classical wave propagation through the medium, and the energy transfer is almost completely due to the macro-scale degree of freedom.

Similar to the case where second gradient terms are small, for the case of large second gradient terms, energy transfer for small wavenumbers in the optical and acoustic waves are governed mainly by means of micro and macro-scale degrees of freedom, respectively. As shown in Fig. 6, for a material with dominant second gradient terms, this behavior continues for higher wavenumbers as well, which is in contrast to the case of small second gradient terms, where the energy transfer at the micro-scale tends to disappear and be replaced by macro-scale mechanisms or vice versa. This decoupling effect in transferring energy in the optical and acoustic branches becomes more significant for smaller values of  $\gamma_4$  and larger values of  $\gamma_1$ .

## 3.3. Special Cases

For a purely second gradient material, following [30], we begin from the internal potential energy expression and assume  $\psi_{ij} = \overline{\phi}_{i,j}$ , followed by the variational approach to obtain the governing

equations of motion. Solving for the wave propagation, thereafter, leads to a dispersion curve in which only one acoustic wave exists. At small wavenumbers, the wave has group velocity of  $\sqrt{1-\gamma_A^2}$ , and at large wavenumbers, it follows the asymptote  $\eta = \gamma_1 \xi$ . Therefore, band gaps do not exist in second gradient materials. It is noteworthy to mention that one cannot reduce Eq. (29) to obtain a second gradient material model. Reducing Eq. (29) to obtain the equations of motion for a second gradient material by assuming  $\psi_{11} = \overline{\phi}_{1,1}$  leads to a dispersion relation for which solving the equation gives rise to two acoustic waves.

To retrieve the classical wave dispersion relation, we assume  $\gamma_A = 0$  and  $\gamma_1 = 0$  in Eq. (38). The result is

$$\eta = \xi \,, \tag{46}$$

which is the non-dispersive relation between the frequency and wavenumber in their dimensionless form. For this case, there is only one acoustic wave and frequency bandgaps are not possible.

# 4. Transverse wave propagation in a one dimensional isotropic continuum with a two dimensional granular micro-structure

#### 4.1. Mathematical Formulation

We now turn our focus on the propagation of a transverse wave in a one dimensional isotropic continuum lying along  $x_2$  axis, with a two dimensional micro-structure in  $x_1'$  and  $x_2'$  directions. A schematic of the general problem is depicted in Fig. 7. Note again that a 1D homogenous isotropic continuum can be, in general, non-homogenous in the RVE (micro-scale). This inhomogeneity may come from the mass density distribution, or the variation of grain pair interaction in the medium. The former is depicted in Fig. 7, while the latter is rather difficult to picturize. As the underlying assumption for deriving Eq. (31) is having a constant  $\rho'$ , our focus in this section is inhomogeneity in grain-pair interactions. We therefore assume that the nonzero kinematic measures are  $\overline{\phi}_1, \psi_{11}, \psi_{22}, \psi_{12}, \psi_{21}$  which are functions of  $x_2$  and t only. The displacement equations Eq. (28), after omitting the terms with zero coefficients for an isotropic granular material using [6], reduces to the following,

$$(\hat{P} + \hat{Q})\bar{\phi}_{1,22} - \hat{Q}\psi_{12,2} - \hat{F}\psi_{21,2} = \rho_{1,1}.$$

$$(\hat{T} + \hat{U})\psi_{12,22} + (\hat{S} - \hat{U})\psi_{21,22} + \hat{Q}\bar{\phi}_{1,2} - \hat{Q}\psi_{12} - \hat{F}\psi_{21} = I_{1}.$$

$$(\hat{S} - \hat{U})\psi_{12,22} + (\hat{R} + \hat{U})\psi_{21,22} + \hat{F}\bar{\phi}_{1,2} - \hat{F}\psi_{12} - \hat{Q}\psi_{21} = I_{1}.$$

$$(\hat{V}\psi_{11,22} + \hat{S}\psi_{22,22} - \hat{W}\psi_{11} - \hat{Z}\psi_{22} = I_{1}.$$

$$(47)$$

$$\hat{S}\psi_{11,22} + \hat{N}\psi_{22,22} - \hat{Z}\psi_{11} - \hat{W}\psi_{22} = I_{1}.$$

where we have used the symbols 
$$\hat{P} = C^{M}_{1212}$$
,  $\hat{Q} = C^{m}_{1212} = C^{m}_{2121}$ ,  $\hat{F} = C^{m}_{1221} = C^{m}_{2112}$ ,  $\hat{W} = C^{m}_{1111} = C^{m}_{2222}$ ,  $\hat{Z} = C^{m}_{1122} = C^{m}_{2211}$ ,  $\hat{S} = A^{g}_{122122} = A^{g}_{212122} = A^{g}_{212122} = A^{g}_{222112}$ ,  $\hat{R} = A^{g}_{212212}$ ,  $\hat{T} = A^{g}_{122122}$ ,  $\hat{V} = A^{g}_{112112}$ ,  $\hat{V} = A^{g}_{1121122}$ ,  $\hat{V} = A^{g}_{1121122}$ , and  $\hat{I} = \frac{1}{3} \rho' d^2$  for brevity.

Eq. (47) entails two uncoupled systems of equations, the first consisting of degrees of freedom  $\overline{\phi}_1, \psi_{12}, \psi_{21}$ , and the second encompassing  $\psi_{11}$  and  $\psi_{22}$ . Each system needs to be separately evaluated. Transverse displacement in macro-scale, therefore, induces only the shear terms in the micro-scale. Interestingly, and in contrast to the behavior at the macro-scale, a perturbation imposed in  $x_2$  direction on the micro-scale leads to not only a dilatational wave in  $x_2$  direction, but also a longitudinal shear wave in the  $x_2$  direction. We note, though, that the focus of the discussion hereafter will be devoted to only the first system of three coupled equations in Eq. (47).

In this paper, we take all the coefficients in the first three equations in Eq. (47) to be positive. This is equivalent to assuming that the micro-scale stiffnesses introduced in [6] in normal direction are greater than their tangential counterparts. Relaxing such an assumption will result in three different systems of equations, each differing with the others only in the sign of the coefficients  $\hat{S}$  and  $\hat{F}$ , however the form of the results remains the same. By assuming solutions of the form

$$\overline{\phi}_{1} = \overline{\phi}_{1}(x_{2}, t), \quad \psi_{12} = \psi_{12}(x_{2}, t), \quad \psi_{21} = \psi_{21}(x_{2}, t),$$
 (48)

and specializing the solutions in Eq. (48) to plane waves, following [16], we will have

$$\overline{\phi}_{1} = \text{Re}(\hat{A}_{1}i \, e^{i(kx_{2} - \omega t)}), \quad \psi_{12} = \text{Re}(\hat{B}_{12} \, e^{i(kx_{2} - \omega t)}), \quad \psi_{21} = \text{Re}(\hat{B}_{21} \, e^{i(kx_{2} - \omega t)}), \tag{49}$$

where k is the wave number,  $\omega$  is the angular frequency, and  $\hat{A}_1$ ,  $\hat{B}_{12}$ , and  $\hat{B}_{21}$  are the amplitudes of the macro-displacement and two micro-displacement gradients, respectively. Similar to section 3, we use the term "frequency" for  $\omega$  hereafter.

Substituting Eq. (49) in the first three equations in Eq. (47) leads to the following matrix form of the governing equations

$$\begin{bmatrix} \hat{c}_{0}^{2}k^{2} & \hat{c}_{A}^{2}k & \hat{c}_{B}^{2}k \\ \frac{k}{\hat{p}_{1}^{2}} & \frac{\hat{p}_{1}^{2}\left(\hat{c}_{1}^{2}+\hat{c}_{4}^{2}\right)k^{2}+1}{\hat{p}_{1}^{2}} & \frac{\hat{p}_{2}^{2}\left(\hat{c}_{2}^{2}-\hat{c}_{4}^{2}\right)k^{2}+1}{\hat{p}_{2}^{2}} \\ \frac{k}{\hat{p}_{2}^{2}} & \frac{\hat{p}_{2}^{2}\left(\hat{c}_{2}^{2}-\hat{c}_{4}^{2}\right)k^{2}+1}{\hat{p}_{2}^{2}} & \frac{\hat{p}_{1}^{2}\left(\hat{c}_{3}^{2}+\hat{c}_{4}^{2}\right)k^{2}+1}{\hat{p}_{1}^{2}} \end{bmatrix} \begin{bmatrix} \hat{A}_{1} \\ \hat{B}_{12} \\ \hat{B}_{21} \end{bmatrix} = \omega^{2} \begin{bmatrix} \hat{A}_{1} \\ \hat{B}_{12} \\ \hat{B}_{21} \end{bmatrix},$$

$$(50)$$

where we have defined the velocities  $\hat{c}_0$ ,  $\hat{c}_A$ , and  $\hat{c}_B$ , related to the macro- and micro-stiffnesses, velocities,  $\hat{c}_1$ ,  $\hat{c}_2$ ,  $\hat{c}_3$ , and  $\hat{c}_4$ , related to the second gradient stiffnesses, and characteristic times  $\hat{p}_1$  and  $\hat{p}_2$  as

$$\hat{c}_{0}^{2} = \frac{\hat{P} + \hat{Q}}{\rho}, \quad \hat{c}_{A}^{2} = \frac{\hat{Q}}{\rho}, \quad \hat{c}_{B}^{2} = \frac{\hat{F}}{\rho}, \tag{51}$$

$$\hat{c}_1^2 = \frac{\hat{T}}{I}, \quad \hat{c}_2^2 = \frac{\hat{S}}{I}, \quad \hat{c}_3^2 = \frac{\hat{R}}{I}, \quad \hat{c}_4^2 = \frac{\hat{U}}{I},$$
 (52)

$$\hat{p}_1^2 = \frac{I}{\hat{O}}, \quad \hat{p}_2^2 = \frac{I}{\hat{F}}.$$
 (53)

Eq. (50) is an eigenvalue problem with the eigenvalue  $\omega^2$  and the eigenvector comprising the amplitudes of the propagating macro-displacement waves and two micro displacement gradient waves as its entries, respectively. It is beneficial to introduce the dimensionless parameter

$$\chi^2 = \frac{\hat{c}_B^2}{\hat{c}_A^2} = \frac{\hat{p}_1^2}{\hat{p}_2^2} = \frac{\hat{F}}{\hat{Q}},\tag{54}$$

which is the ratio of the material parameters  $\hat{F}$  and  $\hat{Q}$ . In order to have an at least semi positive definite energy expression, we must have  $\chi \leq 1$ .

We also introduce the dimensionless velocities as follows

$$\hat{\gamma}_{A}^{2} = \frac{\hat{c}_{A}^{2}}{\hat{c}_{0}^{2}}, \quad \hat{\gamma}_{1}^{2} = \frac{\hat{c}_{1}^{2}}{\hat{c}_{0}^{2}}, \quad \hat{\gamma}_{2}^{2} = \frac{\hat{c}_{2}^{2}}{\hat{c}_{0}^{2}}, \quad \hat{\gamma}_{3}^{2} = \frac{\hat{c}_{3}^{2}}{\hat{c}_{0}^{2}}, \quad \hat{\gamma}_{4}^{2} = \frac{\hat{c}_{4}^{2}}{\hat{c}_{0}^{2}}.$$

$$(55)$$

Using Eq. (54), Eq. (55), and dimensionless wavenumber and frequency

$$\hat{\xi} = \hat{p}_2 \hat{c}_0 k, \quad \hat{\eta} = \hat{p}_2 \omega, \tag{56}$$

we can write the characteristic equation of Eq. (50) as follows

$$\hat{\eta}^{2} = \hat{\xi}^{2} \left( 1 - \hat{\gamma}_{A}^{2} \left( 1 - \chi^{4} \left( 1 + 2\hat{\xi}^{2} \left( \hat{\gamma}_{2}^{2} - \hat{\gamma}_{4}^{2} \right) \right) \right) \right)$$

$$- \chi^{4} \left( \hat{\eta}^{2} - \hat{\xi}^{2} \right) \left( \hat{\eta}^{2} - \left( \hat{\gamma}_{1}^{2} + \hat{\gamma}_{4}^{2} \right) \hat{\xi}^{2} \right) \left( \hat{\eta}^{2} - \left( \hat{\gamma}_{3}^{2} + \hat{\gamma}_{4}^{2} \right) \hat{\xi}^{2} \right)$$

$$+ \chi^{2} \left( \hat{\eta}^{2} - \hat{\xi}^{2} \right) \left( \hat{\eta}^{2} - \left( \hat{\gamma}_{3}^{2} + \hat{\gamma}_{4}^{2} \right) \hat{\xi}^{2} \right) + \chi^{2} \left( \hat{\eta}^{2} - \hat{\xi}^{2} \right) \left( \hat{\eta}^{2} - \left( \hat{\gamma}_{1}^{2} + \hat{\gamma}_{4}^{2} \right) \hat{\xi}^{2} \right)$$

$$+ \chi^{4} \left( \hat{\eta}^{2} - \hat{\xi}^{2} \right) \left( \left( \hat{\gamma}_{2}^{2} - \hat{\gamma}_{4}^{2} \right) \hat{\xi}^{2} + 1 \right)^{2} + \chi^{6} \hat{\gamma}_{A}^{2} \hat{\xi}^{2} \left( \hat{\eta}^{2} - \left( \hat{\gamma}_{1}^{2} + \hat{\gamma}_{4}^{2} \right) \hat{\xi}^{2} \right)$$

$$+ \chi^{2} \hat{\gamma}_{A}^{2} \hat{\xi}^{2} \left( \hat{\eta}^{2} - \left( \hat{\gamma}_{3}^{2} + \hat{\gamma}_{4}^{2} \right) \hat{\xi}^{2} \right).$$

$$(57)$$

Eq. (57) is the general dispersion relation for the considered problem. Concurrent or hierarchical micro-structures result in rather similar dispersion relations and have been studied in [3]. Although the form of the dispersion relation has similarities in terms of the order of the equation, the physics here addresses shear wave in a 1D granular medium with a 2D micro-structure. We note that for the case of  $\psi_{21} = 0$ , the matrix in Eq. (50) reduces to a two by two matrix and leads to the physics of the transverse wave propagation in a one dimensional continuum with one dimensional micro-structure, which is similar in form to the previous problem of longitudinal wave propagation in a one dimensional continuum.

It is useful to include the relation between the parameters  $\hat{T}$ ,  $\hat{S}$ , and  $\hat{R}$ , since all three, for an isotropic granular material, are linear functions of  $K_n^g$  and  $K_w^g$ , according to [6]. Solving for  $\hat{R}$ , and using Eq. (52) and Eq. (55) yields:

$$\hat{\gamma}_3^2 = \frac{1}{3}\hat{\gamma}_1^2 + \frac{2}{3}\hat{\gamma}_2^2. \tag{58}$$

Similar to the approach taken in section 3, we introduce the parameters

$$\hat{B}'_{12} = \hat{p}_2 \hat{c}_0 \hat{B}_{12}, \quad \hat{B}'_{21} = \hat{p}_2 \hat{c}_0 \hat{B}_{21}, \tag{59}$$

and the dimensionless parameters

$$\hat{\beta}_{12} = \frac{\hat{B}'_{12}}{\hat{A}_{1}}, \quad \hat{\beta}_{21} = \frac{\hat{B}'_{21}}{\hat{A}_{1}}. \tag{60}$$

Then, using rows 1 and 2 of the matrix in Eq. (50), Eq. (59), and Eq. (60), we can write

$$\hat{\beta}_{12} = \frac{\left(\hat{\xi}^{2}\left(\hat{\gamma}_{2}^{2} - \hat{\gamma}_{4}^{2}\right) + 1\right)\left(\hat{\eta}^{2} - \hat{\xi}^{2}\right) + \hat{\xi}^{2}\hat{\gamma}_{A}^{2}}{\chi^{2}\hat{\gamma}_{A}^{2}\hat{\xi}\hat{\eta}^{2} + \hat{\gamma}_{A}^{2}\hat{\xi}^{3}\left(\hat{\gamma}_{2}^{2} - \hat{\gamma}_{4}^{2} - \chi^{2}\left(\hat{\gamma}_{1}^{2} + \hat{\gamma}_{4}^{2}\right)\right)},$$

$$\hat{\beta}_{21} = \frac{\left(\chi^{2}\hat{\eta}^{2} - \chi^{2}\hat{\xi}^{2}\left(\hat{\gamma}_{1}^{2} + \hat{\gamma}_{4}^{2}\right) - 1\right)\left(\hat{\eta}^{2} - \hat{\xi}^{2}\right) - \hat{\gamma}_{A}^{2}\hat{\xi}^{2}}{\chi^{4}\hat{\gamma}_{A}^{2}\hat{\xi}\hat{\eta}^{2} + \chi^{2}\hat{\gamma}_{A}^{2}\hat{\xi}^{3}\left(\hat{\gamma}_{2}^{2} - \hat{\gamma}_{4}^{2} - \chi^{2}\left(\hat{\gamma}_{1}^{2} + \hat{\gamma}_{4}^{2}\right)\right)}.$$
(61)

The energy transfer ratio due to the micro- and macro-scale degrees-of-freedom,  $\psi_{12}$ ,  $\psi_{21}$ , and  $\phi_1$ , to the total energy, similar to the approach taken in section 3, can be found, respectively, as

$$\begin{split} \frac{E_{v_{12}}}{E_{total}} &= \\ \frac{\chi^2 \hat{\gamma}_A^2 \hat{\eta}^2 \hat{\beta}_{12}^2 + \hat{\gamma}_A^2 \left(1 + \chi^2\right) \hat{\beta}_{12}^2 + \chi^2 \hat{\gamma}_A^2 \left(\hat{\gamma}_1^2 + \hat{\gamma}_2^2 + 2\hat{\gamma}_4^2\right) \hat{\xi}^2 \hat{\beta}_{12}^2}{\hat{\gamma}_A^2 \left(\chi^2 \hat{\eta}^2 + 1 + \chi^2\right) \left(\hat{\beta}_{12}^2 + \hat{\beta}_{21}^2\right) + \chi^2 \hat{\gamma}_A^2 \left(\hat{\gamma}_1^2 + \hat{\gamma}_2^2 + 2\hat{\gamma}_4^2\right) \hat{\xi}^2 \hat{\beta}_{12}^2 + \chi^2 \hat{\gamma}_A^2 \left(\frac{1}{3} \hat{\gamma}_1^2 + \frac{5}{3} \hat{\gamma}_2^2 + 2\hat{\gamma}_4^2\right) \hat{\xi}^2 \hat{\beta}_{21}^2 + \hat{\eta}^2 + \hat{\xi}^2 \left(1 - \hat{\gamma}_A^2\right)}, \\ \frac{E_{v_{21}}}{E_{total}} &= \\ \frac{\chi^2 \hat{\gamma}_A^2 \hat{\eta}^2 \hat{\beta}_{21}^2 + \hat{\gamma}_A^2 \left(1 + \chi^2\right) \hat{\beta}_{21}^2 + \chi^2 \hat{\gamma}_A^2 \left(\frac{1}{3} \hat{\gamma}_1^2 + \frac{5}{3} \hat{\gamma}_2^2 + 2\hat{\gamma}_4^2\right) \hat{\xi}^2 \hat{\beta}_{21}^2}{\hat{\xi}^2 \hat{\beta}_{21}^2 + \chi^2 \hat{\gamma}_A^2 \left(\hat{\beta}_{12}^2 + \hat{\gamma}_A^2 + 2\hat{\gamma}_A^2\right) \hat{\xi}^2 \hat{\beta}_{21}^2}, \\ \frac{E_{w_{21}}}{\hat{\gamma}_A^2 \left(\chi^2 \hat{\eta}^2 + 1 + \chi^2\right) \left(\hat{\beta}_{12}^2 + \hat{\beta}_{21}^2\right) + \chi^2 \hat{\gamma}_A^2 \left(\hat{\gamma}_1^2 + \hat{\gamma}_2^2 + 2\hat{\gamma}_4^2\right) \hat{\xi}^2 \hat{\beta}_{12}^2 + \chi^2 \hat{\gamma}_A^2 \left(\frac{1}{3} \hat{\gamma}_1^2 + \frac{5}{3} \hat{\gamma}_2^2 + 2\hat{\gamma}_4^2\right) \hat{\xi}^2 \hat{\beta}_{21}^2 + \hat{\eta}^2 + \hat{\xi}^2 \left(1 - \hat{\gamma}_A^2\right)}, \\ \frac{E_{macro}}{E_{total}} &= \\ \frac{\hat{\eta}^2 + \hat{\xi}^2 \left(1 - \hat{\gamma}_A^2\right)}{\hat{\gamma}_A^2 \left(\chi^2 \hat{\eta}^2 + 1 + \chi^2\right) \left(\hat{\beta}_{12}^2 + \hat{\beta}_{21}^2\right) + \chi^2 \hat{\gamma}_A^2 \left(\hat{\gamma}_1^2 + \hat{\gamma}_2^2 + 2\hat{\gamma}_4^2\right) \hat{\xi}^2 \hat{\beta}_{12}^2 + \chi^2 \hat{\gamma}_A^2 \left(\frac{1}{3} \hat{\gamma}_1^2 + \frac{5}{3} \hat{\gamma}_2^2 + 2\hat{\gamma}_4^2\right) \hat{\xi}^2 \hat{\beta}_{21}^2 + \hat{\eta}^2 + \hat{\xi}^2 \left(1 - \hat{\gamma}_A^2\right)}. \\ (63) \end{aligned}$$

## 4.2. Results

Similar to section 3, it is easy to verify that  $\hat{\gamma}_A$  has lower bound limit of 0 and upper bound limit of 1. Very small values of  $\hat{\gamma}_A$  represent materials in which the micro-stiffness in the corresponding direction is negligible compared to their macro-stiffness, and values close to the upper bound level have large micro-stiffness compared to their macro-stiffness. A value of  $\hat{\gamma}_A = 0.71$  corresponds to approximately equal macro- and micro-stiffness of the material.  $\chi$  represents the ratio of the micro-scale stiffness in the two directions considered here, and takes values zero to one. On the other hand,  $\hat{\gamma}_1$ ,  $\hat{\gamma}_2$ ,  $\hat{\gamma}_3$ , and  $\hat{\gamma}_4$  have lower bound of 0, with an upper bound that theoretically can tend to infinity. For a particular ratio of macro-density to micro-inertia, larger  $\hat{\gamma}_i$ , i=1,2,3,4 implies a growing dominance of second gradient behavior. Fig. 8 illustrates the dispersion curves, phase, and group velocities for different values of  $\gamma_A$ ,  $\gamma_1$ ,  $\gamma_2$ ,  $\gamma_4$ , and  $\chi$ , and Fig. 9 shows the energy transfer ratio for the active degrees of freedom here to the total energy transferred by the particular branch under study for the same parameters used in Fig. 8.

Solving the dispersion relation Eq. (57) for the dimensionless frequency,  $\hat{\eta}$ , generally results in three wave branches in the dispersion curve, one acoustic branch, one optical branch, and a third branch. The third branch is an optical branch when  $\chi < 1$  (Fig. 8(a) and Fig. 8(c)) and becomes an acoustic wave when  $\chi = 1$  (Fig. 8(b)). The dimensionless frequencies at which the wave branches start, for the acoustic, optical, and the third branch are  $\hat{\eta} = 0$ ,  $\hat{\eta} = \frac{\sqrt{1 + \chi^2}}{\chi}$ , and  $\hat{\eta} = \frac{\sqrt{1 - \chi^2}}{\chi}$ , respectively.

At small wavenumbers, the acoustic wave has dimensionless group velocity of  $\sqrt{1-\hat{\gamma}_A^2}$  (corresponding to the group velocity of  $\sqrt{\hat{c}_0^2-\hat{c}_A^2}$ ), while the optical wave has dimensionless group velocity of 0. The third branch has 0 and a value of  $\frac{\sqrt{2\hat{\gamma}_1^2-4\hat{\gamma}_2^2+2\hat{\gamma}_3^2+4\hat{\gamma}_4^2}}{2}$  as its dimensionless group velocity at the small wavenumbers when  $\chi < 1$  and  $\chi = 1$ , respectively. Moreover, the asymptotes of the dispersion curves for the acoustic wave, optical wave, and the third wave at large wavenumbers are

$$\hat{\eta} = \frac{1}{2} \sqrt{2 \left( \hat{\gamma}_{1}^{2} + \hat{\gamma}_{3}^{2} + 2 \hat{\gamma}_{4}^{2} \right) - 2 \sqrt{\left( \hat{\gamma}_{1}^{2} - \hat{\gamma}_{3}^{2} \right)^{2} + 4 \left( \hat{\gamma}_{2}^{2} - \hat{\gamma}_{4}^{2} \right)^{2}}} \hat{\xi};$$

$$\hat{\eta} = \hat{\xi};$$

$$\hat{\eta} = \frac{1}{2} \sqrt{2 \left( \hat{\gamma}_{1}^{2} + \hat{\gamma}_{3}^{2} + 2 \hat{\gamma}_{4}^{2} \right) + 2 \sqrt{\left( \hat{\gamma}_{1}^{2} - \hat{\gamma}_{3}^{2} \right)^{2} + 4 \left( \hat{\gamma}_{2}^{2} - \hat{\gamma}_{4}^{2} \right)^{2}}} \hat{\xi}.$$
(64)

Frequency band gaps may appear when the starting point of the optical branches are large dimensionless frequencies, and when group velocities of the acoustic branches at small and large wavenumbers are of small values. There also cases (e.g. Fig. 8(c)) that the real part of the frequency solution of the acoustic branch reduces to zero after a certain wavenumber for a special combination of the material parameters. In this case, there is a region for which the sign of the group velocity for the acoustic branch becomes negative and the peak of the pulse propagates backwards, but the energy flow is always forward [31]. Interestingly, negative group velocity (NGV) occurs for those cases in which the asymptotic dimensionless frequency solution for the acoustic branch given in Eq. (64) takes imaginary values or

$$\hat{\gamma}_1^4 + 2\hat{\gamma}_1^2\hat{\gamma}_2^2 + 4\hat{\gamma}_1^2\hat{\gamma}_4^2 - 3\hat{\gamma}_2^4 + 8\hat{\gamma}_2^2\hat{\gamma}_4^2 < 0, \tag{65}$$

which for the solutions shown in Fig. 8(c) for the noted material parameters corresponds to dimensionless wavenumber ~1.5. Inequality in Eq. (65), can be further expressed in terms of grain-pair second gradient stiffnesses introduced in [6] as follows

$$4(3K_n^g + 4K_w^g)(G_n^u + 4G_w^u) + 3K_w^g(4K_n^g + 3K_w^g) < 0.$$
(66)

which indicates that the condition for NGV occurrence coincides with the requirement for some negative grain-pair second gradient stiffnesses. Grain-pair mechanism which would lead to such conditions are conceivable for granular systems in which the first gradient approximation overestimates the grain-pair deformation energy, such as those in which grain-pair can have large relative shear displacement with low deformation energy caused by small resistance to relative rotations. In addition, it is noteworthy that the overall positive definiteness of energy for the RVE admits the possibility of negative grain-pair second gradient stiffnesses. Such a possibility is surely tantalizing and needs to be further explored with the viewpoint of realizing such granular systems. Further, the inequality in Eq. (65) can be recast, by assuming  $\hat{\gamma}_2 \neq 0$  and introducing the ratios

$$\Upsilon_{12} = \frac{\hat{\gamma}_1}{\hat{\gamma}_2}$$
, and  $\Upsilon_{42} = \frac{\hat{\gamma}_4}{\hat{\gamma}_2}$ , in the form

$$\left(\Upsilon_{12}^2 + 4\Upsilon_{42}^2\right)\left(\Upsilon_{12}^2 + 2\right) - 3 < 0, \tag{67}$$

such that, NGV occurs when Eq. (67) is satisfied. Fig. 10 shows the set of parameters  $\Upsilon_{12}$  and  $\Upsilon_{42}$ , for which the NGV arises. In this figure, white region indicates the sets of parameters for which NGV occurs, and the green color indicates the sets of parameters for which there is no NGV in the acoustic branch. It is noteworthy that NGVs for deformation waves in solids have also been predicted for longitudinal waves in materials with multi-scale micro-structures whose material properties satisfy certain conditions [32]. Finally, we remark that at higher wavenumbers (beyond dimensionless wavenumber  $\sim$ 3.4 in Fig. 8(c)), the frequency solution for the acoustic branch becomes purely imaginary and positive indicating instability.

According to Fig. 9, the energy transferred by the optical wave branch (solid line) is mainly due to micro-scale degrees of freedom at small wavenumbers, and as the wavenumber increases the

role of the macro-scale degree of freedom becomes apparent. In the cases where there is only one acoustic branch, the acoustic branch (dashed line) transfers energy by a mechanism largely due to the macro-scale degree of freedom for small wavenumbers, and as the wavenumber increases, the role that the micro-scale degrees of freedom play becomes dominant. A difference between the proportions of energy each microstructural degree of freedom transfers pertains to the value of the parameter  $\chi$  as it plays the role of a weighting factor for the terms involved in Eq. (54). In the case when  $\chi = 1$  in Fig. 9(b), the acoustic branch reveals a different behavior. In this case, energy is transferred completely by the micro-scale degrees of freedom and the macro-scale degree of freedom plays no role. When  $\chi < 1$  (Fig. 9(a) and Fig. 9(c)), the third branch transfers energy mostly due to the micro-scale degrees of freedom in the ranges where wavenumber is small. This follows by an increase in macro-scale degree of freedom share of energy transfer, and eventually at large wavenumbers, the micro-scale degrees of freedom take over as the degree of freedom  $\psi_{21}$ becomes dominant. In the case of  $\chi = 1$ , the third branch acts as an acoustic branch and the energy transfer mechanism for such branch follows the behavior of acoustic branch in the case of  $\chi < 1$ , except for the large wavenumber behavior in which the degree of freedom  $\psi_{21}$  plays the dominant part.

### 4.3. Special Cases

To model a material with negligible second gradient terms, Eq. (57) reduces to

$$\hat{\eta}^2 = \hat{\xi}^2 \left( 1 - \hat{\gamma}_A^2 \left( 1 - \chi^4 \right) \right) + \chi^2 \left( \hat{\eta}^2 - \hat{\xi}^2 \right) \left( \chi^2 - \chi^2 \hat{\eta}^4 + 2\hat{\eta}^2 \right) + \hat{\gamma}_A^2 \hat{\xi}^2 \hat{\eta}^2 \chi^2 \left( 1 + \chi^4 \right). \tag{68}$$

The parameter  $\chi$  defined in Eq. (54) relates the two material constants  $\hat{F}$  and  $\hat{Q}$  which themselves are functions of  $K_n^m$  and  $K_w^m$  using [6]. Therefore,  $\chi$  can be rewritten as

$$\chi = 1 - \frac{5K_w^m}{K_n^m + 4K_w^m}. (69)$$

Taking into consideration the assumption made earlier in this section,  $K_n^m \ge K_w^m$ , it is seen that  $\chi$  reaches the value 0 when  $K_w^m = K_n^m$  and takes the value 1 only when  $K_w^m = 0$ . In the case of  $K_w^m \ne 0$ , Eq. (68) can be further simplified, by assuming that  $\chi^4$  is negligible, to give

$$\hat{\eta}^2 = \hat{\xi}^2 \left( 1 - \hat{\gamma}_A^2 \right) + 2\hat{\eta}^2 \chi^2 \left( \hat{\eta}^2 - \hat{\xi}^2 \right) + \hat{\gamma}_A^2 \hat{\xi}^2 \hat{\eta}^2 \chi^2 . \tag{70}$$

Eq. (70) has two solutions where one of the solutions is a wave propagating with negligible value for its dimensionless group velocity. Therefore, neglecting the mentioned solution, we can reduce the dispersion relation Eq. (70) to

$$\hat{\eta}^2 = \hat{\xi}^2 \left( 1 - \hat{\gamma}_A^2 \right),\tag{71}$$

which is a non-dispersive acoustic wave with constant phase and group velocity of  $\sqrt{\hat{c}_0^2 - \hat{c}_A^2}$ .

In the case where  $K_w^m = 0$ , Eq. (68) reduces to

$$\hat{\eta}^2 = \hat{\xi}^2 + (\hat{\eta}^2 - \hat{\xi}^2)(1 - \hat{\eta}^4 + 2\hat{\eta}^2) + 2\hat{\gamma}_A^2 \hat{\xi}^2 \hat{\eta}^2, \tag{72}$$

which gives rise to one standing (evanescent) wave, one acoustic wave that reaches zero group velocity as wavenumber increases, and one optical wave with an asymptote of  $\hat{\eta} = \hat{\xi}$ .

For the case in which the second gradient terms are large,  $\hat{\gamma}_A$  is negligible, and  $\chi = 1$ , one must start from Eq. (47) and let  $\hat{Q} = \hat{F} = 0$ . Solution includes three wave branches of

$$\omega = \hat{c}_{0}k,$$

$$\omega = \frac{1}{2}\sqrt{2(\hat{c}_{1}^{2} + \hat{c}_{3}^{2} + 2\hat{c}_{4}^{2}) + 2\sqrt{(\hat{c}_{1}^{2} - \hat{c}_{3}^{2})^{2} + 4(\hat{c}_{2}^{2} - \hat{c}_{4}^{2})^{2}}}k,$$

$$\omega = \frac{1}{2}\sqrt{2(\hat{c}_{1}^{2} + \hat{c}_{3}^{2} + 2\hat{c}_{4}^{2}) - 2\sqrt{(\hat{c}_{1}^{2} - \hat{c}_{3}^{2})^{2} + 4(\hat{c}_{2}^{2} - \hat{c}_{4}^{2})^{2}}}k.$$
(73)

According to Eq. (73), the first solution is a classical wave with the constant velocity  $\hat{c}_0$  depending on the macro-scale properties which propagates as an acoustic wave. Second and third solutions

are also acoustic waves having constant velocities with the third branch only existing when the expression under the square root is positive, which is simplified to

$$\hat{c}_1^4 + 2\hat{c}_1^2\hat{c}_2^2 + 4\hat{c}_1^2\hat{c}_4^2 - 3\hat{c}_2^4 + 8\hat{c}_2^2\hat{c}_4^2 > 0. \tag{74}$$

Due to its physical nature,  $\hat{c}_4$  is usually negligible compared to the other two parameters involved. Therefore, Eq. (74) reduces to  $\hat{c}_1 > \hat{c}_2$ . As a result, for the cases where  $\hat{c}_2$  is comparatively higher than  $\hat{c}_1$ , an evanescent wave is expected as the third solution of the dispersion equation. Starting from Eq. (57) to obtain the solutions for the dispersive behavior, however, leads to a set of three solutions for which one of the solutions is an optical wave.

For a purely second gradient material, as discussed in section 3, the form of deformation energy must be appropriately specified and the governing equation must be derived applying the variational approach. In this case, only one acoustic wave will exist for the considered problem, whose dispersion relation will be similar to that given in [30].

Finally, assuming that  $\hat{\gamma}_i$ , i = A,1,2,3,4 are negligible and  $\chi = 1$ , Eq. (57) reduces to the dispersion relation for the classical wave equation which has a non-dispersive solution similar to Eq. (46).

# 5. Micromechanical Implications to Metamaterial Design

To illustrate the effects of the inter-granular stiffness coefficients on the behavior of the systems studied, we proceed as follows. We assume, as in sections 3 and 4, that the normal components of the inter-granular stiffness are larger than their corresponding tangential values and they are both nonnegative.

In section 3 of this paper, we discussed the different behavior the system might exhibit based on the values the dimensionless velocities  $\gamma_A$  and  $\gamma_1$  take. We have shown that  $\gamma_A$  is bounded between zero and one, whilst  $\gamma_1$  can take any nonnegative value. Using Eq. (37), and substituting for the material parameters computed in [6] we can write

$$\gamma_{A} = \sqrt{\frac{K_{n}^{m}(3 + 2\Omega^{m})}{K_{n}^{m}(3 + 2\Omega^{m}) + K_{n}^{M}(3 + 2\Omega^{M})}}, \quad \gamma_{1} = \sqrt{\frac{3\rho l^{2}}{7I}} \sqrt{\frac{K_{n}^{g}(5 + 2\Omega^{g})}{K_{n}^{m}(3 + 2\Omega^{m}) + K_{n}^{M}(3 + 2\Omega^{M})}}, \quad (75)$$

where we have introduced ratios of tangential to normal stiffness coefficients as

$$\Omega^M = \frac{K_w^M}{K_n^M}, \quad \Omega^m = \frac{K_w^m}{K_n^m}, \quad \Omega^g = \frac{K_w^g}{K_n^g}. \tag{76}$$

The same approach can also be taken for the dimensionless velocities in the section 4. It is straightforward to see that a specific value of  $\gamma_A$  can be retained if the ratio  $\frac{K_n^M \left(3 + 2\Omega^M\right)}{K_n^m \left(3 + 2\Omega^m\right)}$ 

remains constant. For instance, taking the values of  $\Omega^M$  and  $\Omega^m$  to remain constant,  $\gamma_A$  retains its value provided the ratio  $K_n^M/K_n^m$  is constant (such as for the two sets of  $K_n^M=2, K_n^m=1$ , and  $K_n^M=4, K_n^m=2$ ). The implication is that by changing the micro-stiffness coefficients in certain predefined manner, similar macro-scale phenomena may be achieved. However, these two sets will generate two different values for  $\gamma_1$ , which means that while one part of the phenomena can be preserved, another associated may not.

Furthermore, Eq. (75) proposes that for a given ratio of macro- and micro-inertia, the parameters

$$\gamma_{A} = \gamma_{A}(K_{n}^{m}, K_{n}^{M}, \Omega^{m}, \Omega^{M}), \quad \gamma_{1} = \gamma_{1}(K_{n}^{g}, K_{n}^{m}, K_{n}^{M}, \Omega^{g}, \Omega^{m}, \Omega^{M}),$$
 (77)

are purely functions of stiffnesses associated to the introduced kinematic quantities. It is worthwhile to consider effects arise mainly from elasticity rather than inertia considering that the grain-pair interactions can vary strongly while the grain density, granular structure and RVE size remain virtually similar. Now, according to what has been discussed in section 3, emergence of bandgaps with a certain location and width is dependent on a certain combinations of the parameters  $\gamma_1$  and  $\gamma_A$ . Therefore, to design a structure with a desired bandgap location and width, a multi-objective optimization problem must be posed. The problem becomes more intricate as we increase the dimension of the physics involved and add to the desired properties for the design.

An advantage of the proposed continuum model is the availability of the explicit form of the functions, thereby promising a complete domain to search for possible solutions (see similar approach exemplified for pantographic material systems in [33]). Such theory based approaches are in contrast to certain efforts that proceed by postulating a priori certain predetermined sets of micro-structures [8, 10] or propose to combine micro-elements [34, 35] to achieve an objective that is circumscribed within a known domain of behaviors without the aid of theories that can predict possibilities beyond those that are already known. The optimization problem may be solved using metaheuristic algorithms, such as Genetic Algorithm. There is always possible to have many different combinations of grain-pair stiffnesses yielding the same result, since the expressions for the dimensionless velocities are not one-to-one functions. This means that there is more than one solution to the problem being solved. This is equivalent to stating that many physically different structures can demonstrate similar behavior when excited, and hence, be typified in the same category, and be manufactured based on the existing manufacturing processes and resources. The knowledge obtained from such analyses is particularly useful in the design and fabrication of metamaterials with specific material properties for particular purposes, e.g. to be used as wave attenuators or nanoscale energy harvesting devices, as recent studies on granular crystals have shown [33, 36-39]. The granular micromechanics based continuum model, therefore, suggests, and predicts, that controlling or varying the inter-granular stiffness coefficients and micro-structure results in a material for which the behavior it manifests when undergoing different loading conditions can be tuned, thus providing us with a practical mechanism to make materials with unusual desired behavior. Linking microstructural properties of the material to its macroscopic behavior promises optimizing large scale structures in terms of their stiffness to weight ratios and desired directional properties, which seems infeasible using current approaches such as discrete element methods, namely due to their substantial computational cost. Since the dimensionless speeds are responsible for the way the material behaves when subjected to external actions, and since intergranular stiffness coefficients are the building elements that the dimensionless speeds are functions of, starting from the micro-scale and proceed with a tailored micro-structure with desired stiffness coefficients using novel technological advancements will lead to a material whose behavior is predicted, yet complex and unprecedented, as for instance the predicted granular materials displaying negative group velocities or frequency band gaps.

# 6. Summary and Conclusions

In the present paper, two cases of wave propagation in linear elastic granular continua were studied. Case 1 investigated a longitudinal wave propagating in a one dimensional infinite continuum, while case 2 studied a transverse wave propagating in a one dimensional continuum that has a two dimensional micro-structure. The results obtained are expected to provide a baseline and point of departure for more complex problems that could involve nonlinearities and dissipation. For each case, the effect of parameters involved in the dispersion equations was investigated. For case 1, there are two waves emerging in the dispersion curve, optical and acoustic branches. Results show that the wave speed for both the branches is dictated by the macro- and micro-scale properties for the small and large wavenumbers, respectively. The study on energy transfer mechanism reveals a shift between macro- and micro-scale degrees of freedom for the two branches as the wavenumber increases. Large values of second gradient terms prevent this shift, and therefore, lead to the case where the energy in optical wave is mainly transferred by the microscale degree of freedom, and macro-scale degree of freedom leads the energy transfer in the acoustic wave. For case 2, dispersive behavior of the material gives rise to three wave branches, one acoustic, one optical, and the third branch being acoustic or optical depending on the value of the parameter  $\chi$ . As discussed in the paper, the model proposed in [6] reflects, in a sufficient way, the effect of micro-measures (such as micro-stiffnesses, grain sizes and granular structure) on the macro-scale motion, accounting for frequency band gaps and negative group velocities. The results discussed in this paper show that the connection between the micro-measures and the continuum model can pave a way for exploring the micro-mechanical antecedents of phenomena The granular micromechanics can thus provide the theoretical observed at macro-scales. underpinning and an efficient paradigm for designing granular metamaterials with desired dispersive behavior that may be needed for particular applications. In absence of such a theory, the possibilities of many predicted behavior would remain concealed and undiscovered. Clearly, a more expansive model accounting for the electro-magneto-elasticity of the granular materials [5, 40, 41], or dissipation and damage mechanisms [42, 43] that also takes rotation (spin) of the grains as extra degrees of freedom will reveal more complex features of the granular materials, and hence, will be pursued in following research. Given that experimental procedures for wave propagation in complex granular materials are not easily devised, numerical simulations with discrete models

could be potentially utilized to verify the results presented here. The future work will also consider such discrete models with full dynamic identification procedure between the discrete and continuum models.

# Acknowledgements

This research is supported in part by the United States National Science Foundation grant CMMI -1727433.

#### References

- [1] Bazzaz M, Darabi MK, Little DN, Garg N. A Straightforward Procedure to Characterize Nonlinear Viscoelastic Response of Asphalt Concrete at High Temperatures. Transportation Research Record. 2672(28) (2018) 481-92.
- [2] Misra A, Singh V, Darabi MK. Asphalt pavement rutting simulated using granular micromechanics-based rate-dependent damage-plasticity model. International Journal of Pavement Engineering. (2017) 1-14.
- [3] Berezovski A, Engelbrecht J, Salupere A, Tamm K, Peets T, Berezovski M. Dispersive waves in microstructured solids. International Journal of Solids and Structures. 50(11) (2013) 1981-90.
- [4] Engelbrecht J, Berezovski A, Pastrone F, Braun M. Waves in microstructured materials and dispersion. Philosophical Magazine. 85(33-35) (2005) 4127-41.
- [5] Nejadsadeghi N, Placidi L, Romeo M, Misra A. Frequency Band Gaps in Dielectric Granular Metamaterials Modulated By Electric Field. Mech Res Commun. 95 (2019) 96-103.
- [6] Misra A, Poorsolhjouy P. Granular micromechanics based micromorphic model predicts frequency band gaps. Continuum Mechanics and Thermodynamics. 28(1-2) (2016) 215-34.
- [7] Misra A, Placidi L, Turco E. Variational Methods for Continuum Models of Granular Materials. 2019. p. 1-11.
- [8] Li J, Li S. Generating ultra wide low-frequency gap for transverse wave isolation via inertial amplification effects. Physics Letters A. 382(5) (2018) 241-7.
- [9] Colombi A, Craster RV, Colquitt D, Achaoui Y, Guenneau S, Roux P, et al. Elastic Wave Control Beyond Band-Gaps: Shaping the Flow of Waves in Plates and Half-Spaces with Subwavelength Resonant Rods. Frontiers in Mechanical Engineering. 3(10) (2017).
- [10] An X, Fan H, Zhang C. Elastic wave and vibration bandgaps in two-dimensional acoustic metamaterials with resonators and disorders. Wave Motion. 80 (2018) 69-81.
- [11] dell'Isola F, Maier G, Perego U, Andreaus U, Esposito R, Forest S. The complete works of Gabrio Piola: Volume I: Commented English Translation-English and Italian Edition: Springer International Publishing; 2014. 813 p.
- [12] Eugster SR, dell'Isola F. Exegesis of the Introduction and Sect. I from "Fundamentals of the Mechanics of Continua"\*\* by E. Hellinger. ZAMM-Journal of Applied Mathematics and Mechanics/Zeitschrift für Angewandte Mathematik und Mechanik. 97(4) (2017) 477-506.
- [13] Rosi G, Auffray N. Anisotropic and dispersive wave propagation within strain-gradient framework. Wave Motion. 63 (2016) 120-34.
- [14] Rosi G, Placidi L, Auffray N. On the validity range of strain-gradient elasticity: a mixed static-dynamic identification procedure. European Journal of Mechanics-A/Solids. 69 (2018) 179-91.
- [15] Placidi L, Rosi G, Giorgio I, Madeo A. Reflection and transmission of plane waves at surfaces carrying material properties and embedded in second-gradient materials. Mathematics and Mechanics of Solids. 19(5) (2014) 555-78.
- [16] Mindlin RD. Micro-Structure in Linear Elasticity. Archive for Rational Mechanics and Analysis. 16(1) (1964) 51-78.
- [17] Eringen AC. Microcontinuum field theories: foundations and solids: Springer New York; 1999.
- [18] Engelbrecht J, Berezovski A. Reflections on mathematical models of deformation waves in elastic microstructured solids. Mathematics and Mechanics of Complex Systems. 3(1) (2015) 43-82.

- [19] Pastrone F, Engelbrecht J, editors. Waves and complexity of microstructured solids. 2012 Proceedings of the International Conference Days on Diffraction; 2012 May 28 2012-June 1 2012.
- [20] Misra A, Poorsolhjouy P. Grain- and macro-scale kinematics for granular micromechanics based small deformation micromorphic continuum model. Mech Res Commun. 81 (2017) 1-6.
- [21] Suiker ASJ, de Borst R, Chang CS. Micro-mechanical modelling of granular material. Part 1: Derivation of a second-gradient micro-polar constitutive theory. Acta Mechanica. 149(1-4) (2001) 161-80.
- [22] Suiker ASJ, de Borst R, Chang CS. Micro-mechanical modelling of granular material. Part 2: Plane wave propagation in infinite media. Acta Mechanica. 149(1-4) (2001) 181-200.
- [23] Merkel A, Luding S. Enhanced micropolar model for wave propagation in ordered granular materials. International Journal of Solids and structures. 106 (2017) 91-105.
- [24] Misra A, Poorsolhjouy P. Identification of higher-order elastic constants for grain assemblies based upon granular micromechanics. Mathematics and Mechanics of Complex Systems. 3(3) (2015) 285-308.
- [25] Misra A, Poorsolhjouy P. Elastic Behavior of 2D Grain Packing Modeled as Micromorphic Media Based on Granular Micromechanics. Journal of Engineering Mechanics. 143(1) (2016) C4016005.
- [26] Mindlin R. Micro-structure in linear elasticity. Archive for Rational Mechanics and Analysis. 16(1) (1964) 51-78.
- [27] Misra A, Placidi L, Turco E. Variational Methods for Discrete Models of Granular Materials. In: Altenbach H, Ochsner A, editors. Encyclopedia of Continuum Mechanics: Springer Verlag; 2018.
- [28] Germain P. Method of Virtual Power in Continuum Mechanics .2. Microstructure. Siam Journal on Applied Mathematics. 25(3) (1973) 556-75.
- [29] Peets T. Internal scales and dispersive properties of microstructured materials. Mathematics and Computers in Simulation. 127 (2016) 220-8.
- [30] Madeo A, Neff P, Ghiba I-D, Placidi L, Rosi G. Wave propagation in relaxed micromorphic continua: modeling metamaterials with frequency band-gaps. Continuum Mechanics and Thermodynamics. (2013) 1-20.
- [31] Peets T, Kartofelev D, Tamm K, Engelbrecht J. Waves in microstructured solids and negative group velocity. EPL (Europhysics Letters). 103(1) (2013) 16001.
- [32] Tamm K, Peets T, Engelbrecht J, Kartofelev D. Negative group velocity in solids. Wave Motion. 71 (2017) 127-38.
- [33] dell'Isola F, Seppecher P, Alibert JJ, Lekszycki T, Grygoruk R, Pawlikowski M, et al. Pantographic metamaterials: an example of mathematically driven design and of its technological challenges. Continuum Mechanics and Thermodynamics. (2018) 1-34.
- [34] Matlack KH, Serra-Garcia M, Palermo A, Huber SD, Daraio C. Designing perturbative metamaterials from discrete models. Nature materials. 17(4) (2018) 323.
- [35] Bilal OR, Süsstrunk R, Daraio C, Huber SD. Intrinsically polar elastic metamaterials. Advanced Materials. 29(26) (2017) 1700540.
- [36] Kumar Pal R, Waymel RF, Geubelle PH, Lambros J. Tunable Wave Propagation in Granular Crystals by Altering Lattice Network Topology. Journal of Engineering Materials and Technology. 139(1) (2016) 011005--7.
- [37] Pal RK, Geubelle PH. Wave tailoring by precompression in confined granular systems. Physical review E, Statistical, nonlinear, and soft matter physics. 90(4) (2014) 042204.

- [38] Xu J, Zheng B. Stress Wave Propagation in Two-dimensional Buckyball Lattice. Scientific Reports. 6 (2016) 37692.
- [39] Merkel A, Tournat V, Gusev V. Experimental Evidence of Rotational Elastic Waves in Granular Phononic Crystals. Physical Review Letters. 107(22) (2011).
- [40] Romeo M. Electroelastic waves in dielectrics modeled as polarizable continua. Wave Motion. 60 (2016) 121-34.
- [41] Romeo M. Microcontinuum approach to electromagneto-elasticity in granular materials. Mech Res Commun. 91 (2018) 33-8.
- [42] Misra A, Singh V. Thermomechanics-based nonlinear rate-dependent coupled damage-plasticity granular micromechanics model. Continuum Mechanics and Thermodynamics. 27(4-5) (2014) 787-817.
- [43] Placidi L, Misra A, Barchiesi E. Two-dimensional strain gradient damage modeling: a variational approach. Zeitschrift für angewandte Mathematik und Physik. 69(3) (2018) 56.

## **List of Figures**

- Fig 1. Schematic of the continuum material point, P, and its granular micro-structure magnified for better visualization, where the x' coordinate system is attached to its barycenter.
- Fig. 2. Schematic of a 1D continuum in  $x_1$  direction with granular micro-structure in  $x_1$ ' direction. A material point in the macro-scale coordinate system is itself a collection of grains that can differ in micro-density, micro-morphology and micro-mechanical properties.
- **Fig. 3.** Dispersion curves, and ratio of energy transferred by micro-scale degree of freedom to the total energy for optical and acoustic branches, for different values of  $\gamma_A$  and  $\gamma_1$ , where solid lines and dashed lines represent optical branches and acoustic branches respectively, and lines with  $\ast$ , and  $\square$  represent  $\gamma_1 = 0.0002$ ,  $\gamma_1 = 0.3$ , and  $\gamma_1 = 0.7$ , respectively.
- **Fig. 4.** Dispersion curves, and ratio of energy transferred by micro-scale degree of freedom to the total energy for optical and acoustic branches, for different values of  $\gamma_A$  and  $\gamma_1$ , where solid lines and dashed lines represent optical branches and acoustic branches respectively, and lines with \*,  $\triangle$ , and  $\square$  represent  $\gamma_1 = 1$ ,  $\gamma_1 = 2$ , and  $\gamma_1 = 3$ , respectively.
- **Fig. 5.** Phase velocities  $\upsilon_p$ , and group velocities  $\upsilon_g$ , for optical and acoustic branches, for different values of  $\gamma_A$  and  $\gamma_1$ , where solid lines and dashed lines represent optical branches and acoustic branches respectively, and lines with  $\ast$ ,  $\triangle$ , and  $\square$  represent  $\gamma_1 = 0.0002$ ,  $\gamma_1 = 0.3$ , and  $\gamma_1 = 0.7$ , respectively.
- **Fig. 6.** Phase velocities  $\upsilon_p$ , and group velocities  $\upsilon_g$ , for optical and acoustic branches, for different values of  $\gamma_A$  and  $\gamma_1$ , where solid lines and dashed lines represent optical branches and acoustic branches respectively, and lines with  $\ast$ ,  $\Delta$ , and  $\square$  represent  $\gamma_1 = 1$ ,  $\gamma_1 = 2$ , and  $\gamma_1 = 3$ , respectively.
- Fig. 7. Schematic of a 1D continuum in  $x_2$  direction with granular micro-structure in both  $x_1$ ' and  $x_2$ ' directions. A material point in the macro-scale coordinate system is itself a collection of grains that can differ in micro-density, micro-morphology and micro-mechanical properties.
- **Fig. 8.** Dispersion curves, phase velocities  $v_p$ , and group velocities  $v_g$  for the optical branch, the third branch, and the acoustic branch, respectively, where solid line represents an optical branch,

dash-dotted line represents an acoustic branch, and dashed line is either acoustic or optical (third branch). (a) A material with properties of  $\hat{\gamma}_A = 0.71$ ,  $\hat{\gamma}_1 = 0.5$ ,  $\hat{\gamma}_2 = 0.3$ ,  $\hat{\gamma}_4 = 0.1$ , and  $\chi = 0.8$ ; (b) A material with properties of  $\hat{\gamma}_A = 0.71$ ,  $\hat{\gamma}_1 = 0.5$ ,  $\hat{\gamma}_2 = 0.3$ ,  $\hat{\gamma}_4 = 0.1$ , and  $\chi = 1$ ; (c) A material with properties of  $\hat{\gamma}_A = 0.71$ ,  $\hat{\gamma}_1 = 0.2$ ,  $\hat{\gamma}_2 = 0.4$ ,  $\hat{\gamma}_4 = 0.1$ , and  $\chi = 0.8$ .

**Fig. 9.** Ratio of energy transferred by macro- and micro-scale degrees of freedom to the total energy for the optical branch, the third branch, and the acoustic branch, respectively, where solid line represents an optical branch, dash-dotted line represents an acoustic branch, and dashed line is either acoustic or optical (third branch). Lines with \*,  $\wedge$ , and  $\square$  represent energy transferred by macro-scale degree of freedom  $\phi_1$ , and micro-scale degrees of freedom  $\psi_{21}$  and  $\psi_{12}$ , respectively. (a) A material with properties of  $\hat{\gamma}_A = 0.71$ ,  $\hat{\gamma}_1 = 0.5$ ,  $\hat{\gamma}_2 = 0.3$ ,  $\hat{\gamma}_4 = 0.1$ , and  $\chi = 0.8$ ; (b) A material with properties of  $\hat{\gamma}_A = 0.71$ ,  $\hat{\gamma}_1 = 0.5$ ,  $\hat{\gamma}_2 = 0.3$ ,  $\hat{\gamma}_4 = 0.1$ , and  $\chi = 1$ ; (c) A material with properties of  $\hat{\gamma}_A = 0.71$ ,  $\hat{\gamma}_1 = 0.2$ ,  $\hat{\gamma}_2 = 0.4$ ,  $\hat{\gamma}_4 = 0.1$ , and  $\chi = 0.8$ .

**Fig. 10** White indicates the sets of parameters for which negative group velocity (NGV) occurs in the acoustic branch, while green color indicates the sets of parameters for which there is no NGV.

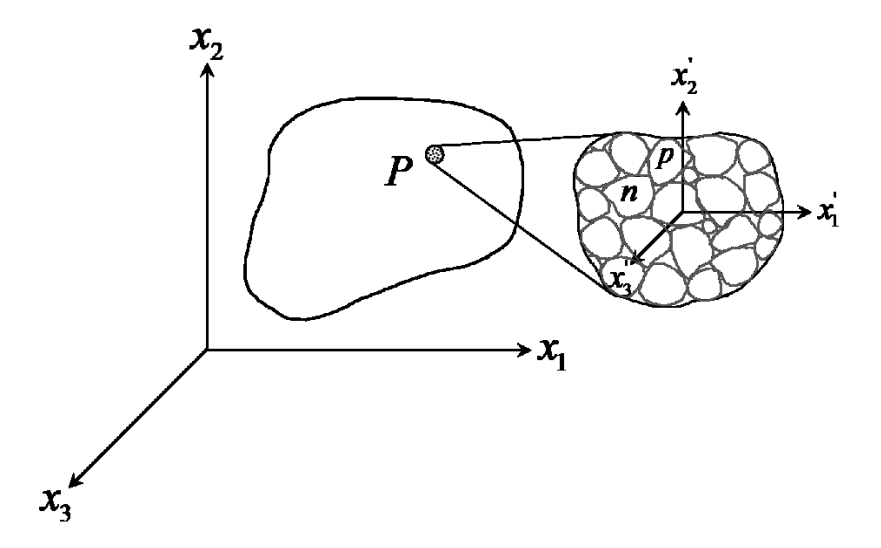


**Fig 1.** Schematic of the continuum material point, P, and its granular micro-structure magnified for better visualization, where the x' coordinate system is attached to its barycenter.

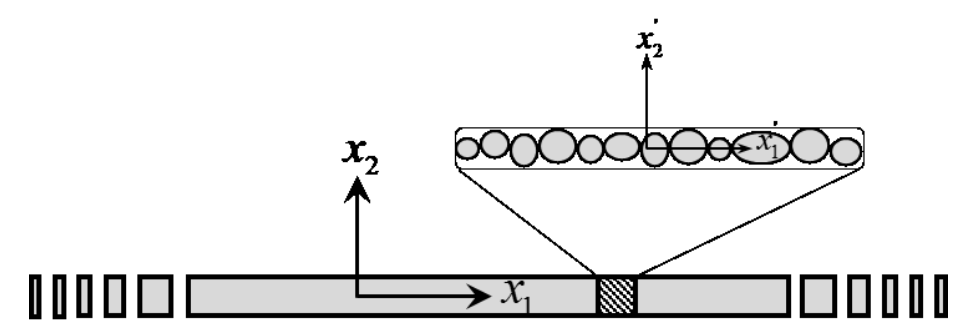


**Fig. 2.** Schematic of a 1D continuum in  $x_1$  direction with granular micro-structure in  $x_1$ ' direction. A material point in the macro-scale coordinate system is itself a collection of grains that can differ in micro-density, micro-morphology and micro-mechanical properties.

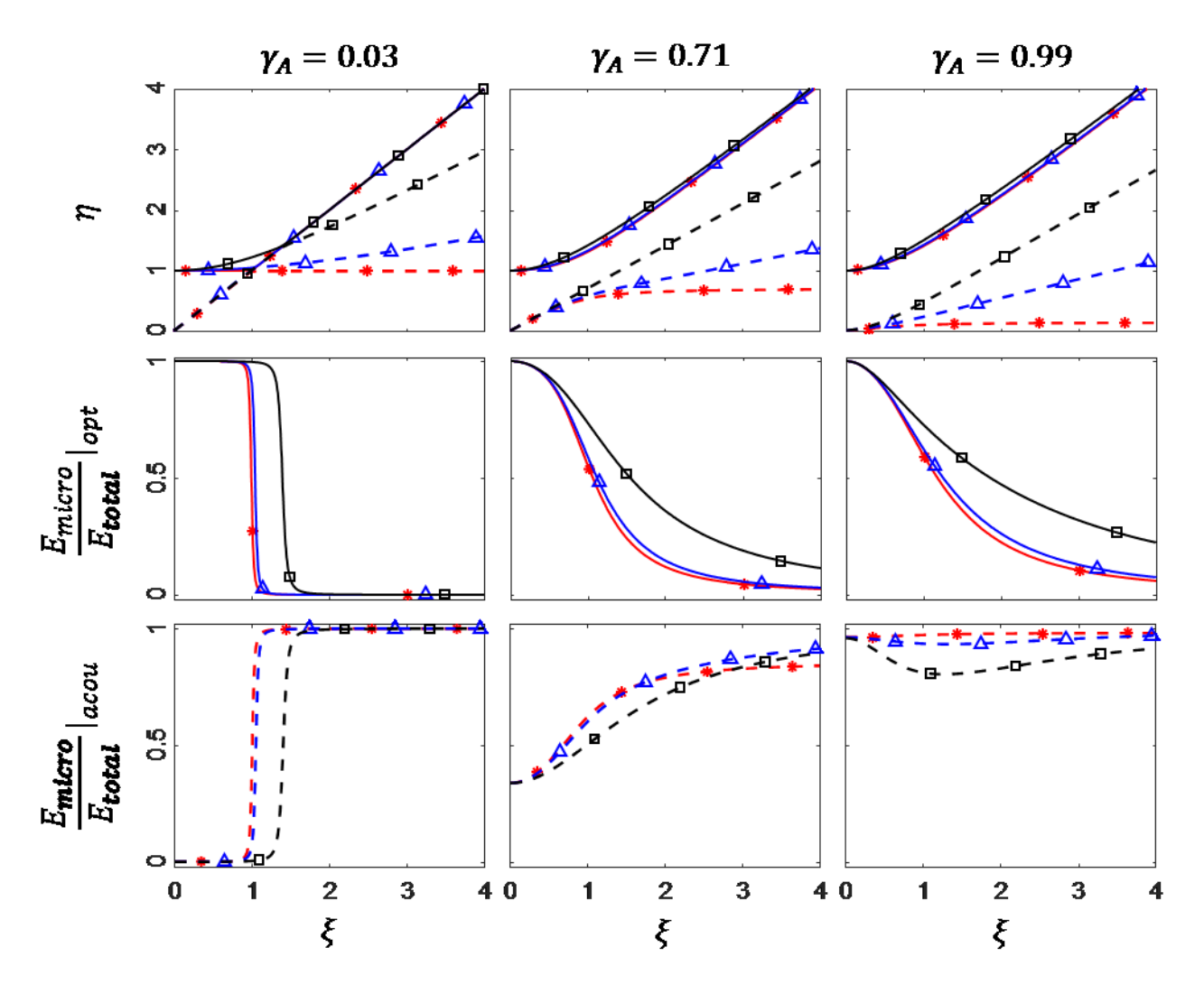


**Fig. 3.** Dispersion curves, and ratio of energy transferred by micro-scale degree of freedom to the total energy for optical and acoustic branches, for different values of  $\gamma_A$  and  $\gamma_1$ , where solid lines and dashed lines represent optical branches and acoustic branches respectively, and lines with \*,  $\Delta$ , and  $\Box$  represent  $\gamma_1 = 0.0002$ ,  $\gamma_1 = 0.3$ , and  $\gamma_1 = 0.7$ , respectively.

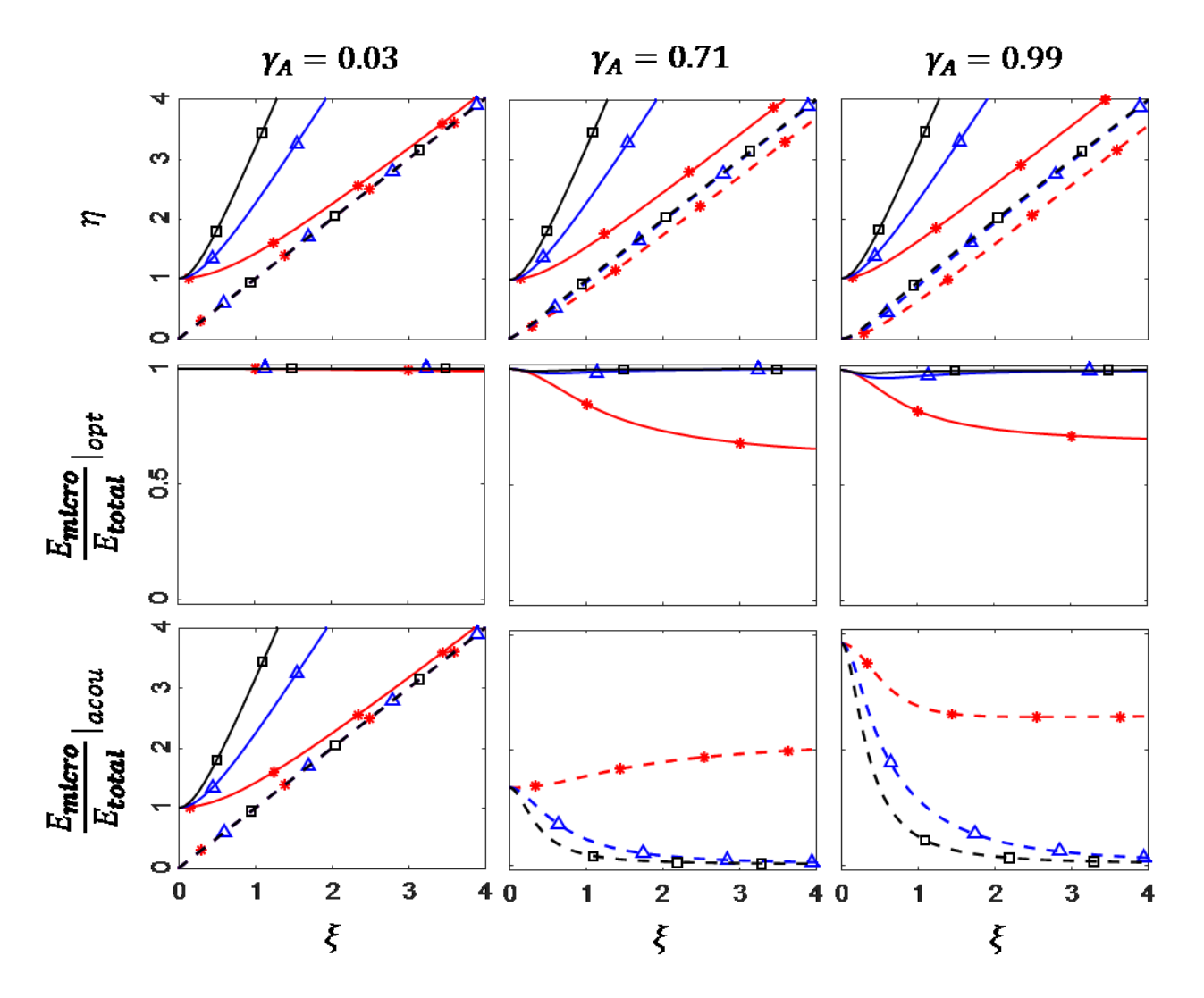


**Fig. 4.** Dispersion curves, and ratio of energy transferred by micro-scale degree of freedom to the total energy for optical and acoustic branches, for different values of  $\gamma_A$  and  $\gamma_1$ , where solid lines and dashed lines represent optical branches and acoustic branches respectively, and lines with \*,  $\triangle$ , and  $\square$  represent  $\gamma_1 = 1$ ,  $\gamma_1 = 2$ , and  $\gamma_1 = 3$ , respectively.

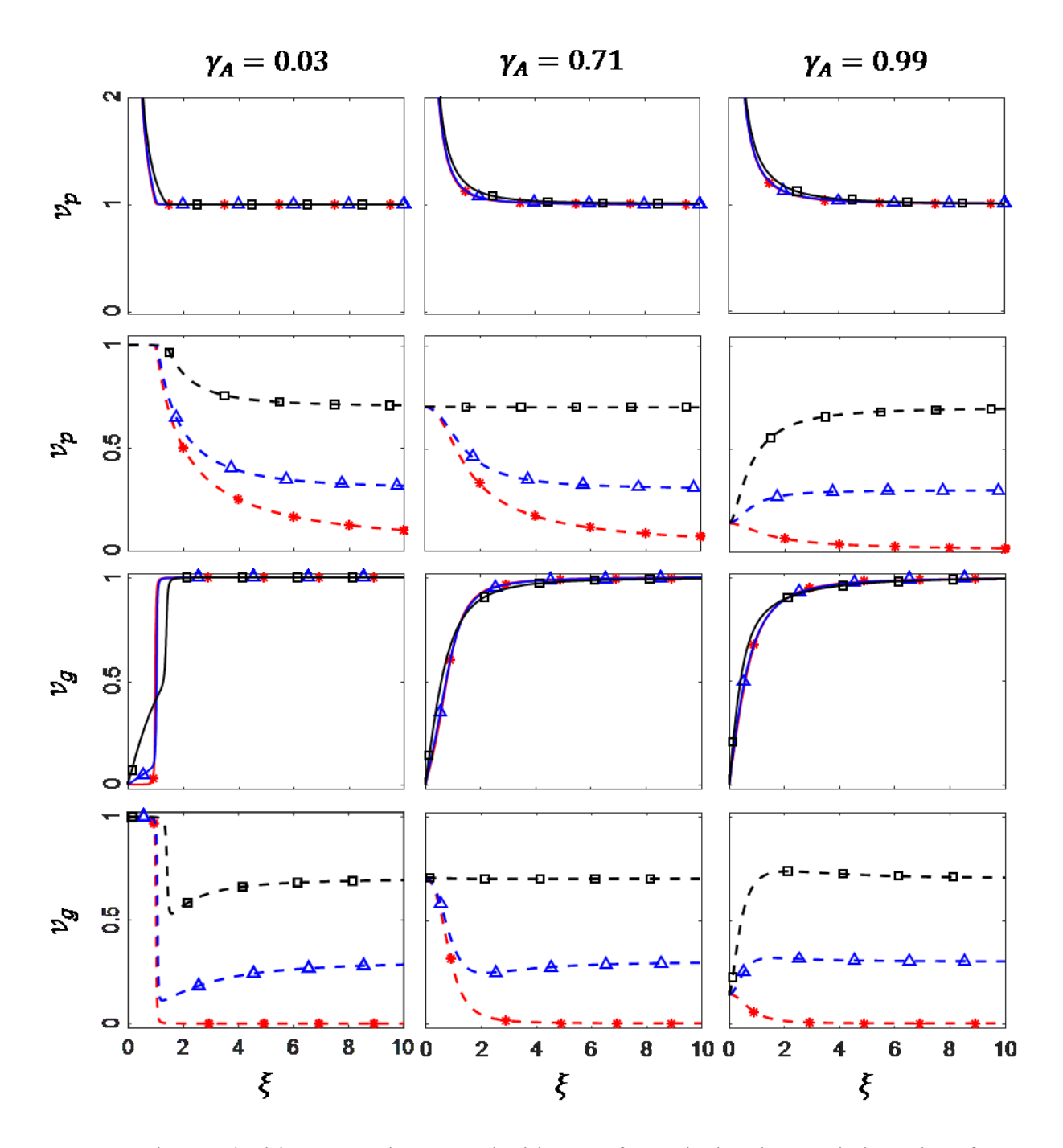
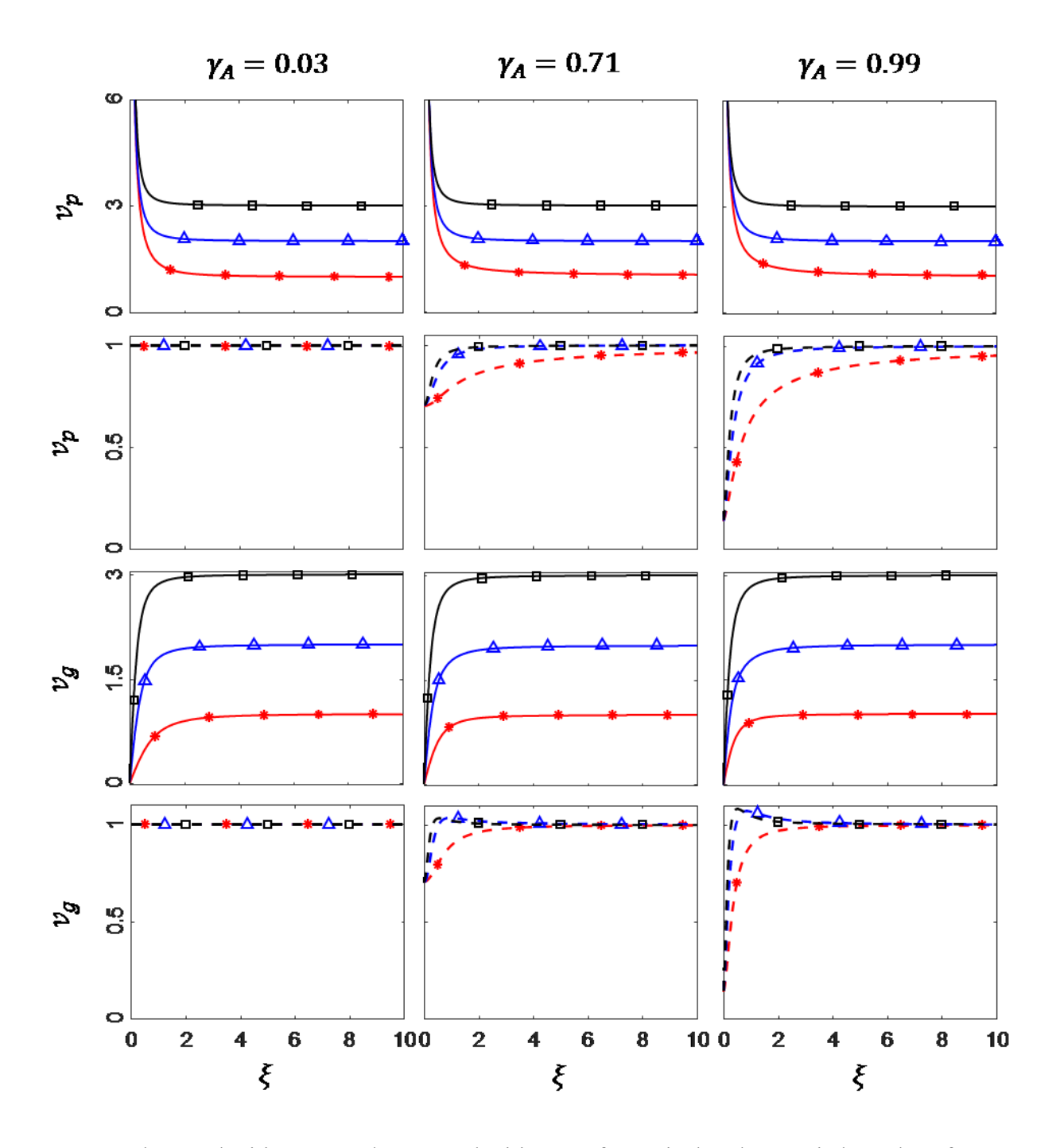


Fig. 5. Phase velocities  $\upsilon_p$ , and group velocities  $\upsilon_g$ , for optical and acoustic branches, for different values of  $\gamma_A$  and  $\gamma_1$ , where solid lines and dashed lines represent optical branches and acoustic branches respectively, and lines with \*,  $\triangle$ , and  $\square$  represent  $\gamma_1 = 0.0002$ ,  $\gamma_1 = 0.3$ , and  $\gamma_1 = 0.7$ , respectively.



**Fig. 6.** Phase velocities  $\upsilon_p$ , and group velocities  $\upsilon_g$ , for optical and acoustic branches, for different values of  $\gamma_A$  and  $\gamma_1$ , where solid lines and dashed lines represent optical branches and acoustic branches respectively, and lines with \*,  $\triangle$ , and  $\square$  represent  $\gamma_1 = 1$ ,  $\gamma_1 = 2$ , and  $\gamma_1 = 3$ , respectively.

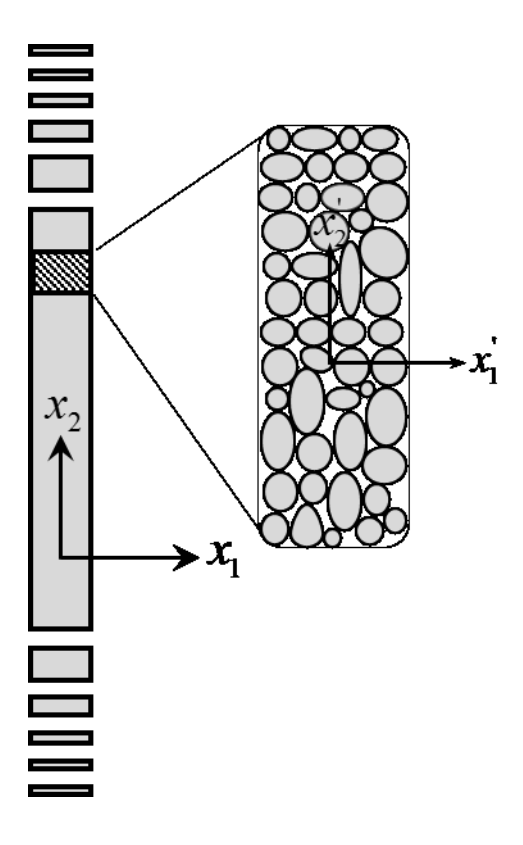
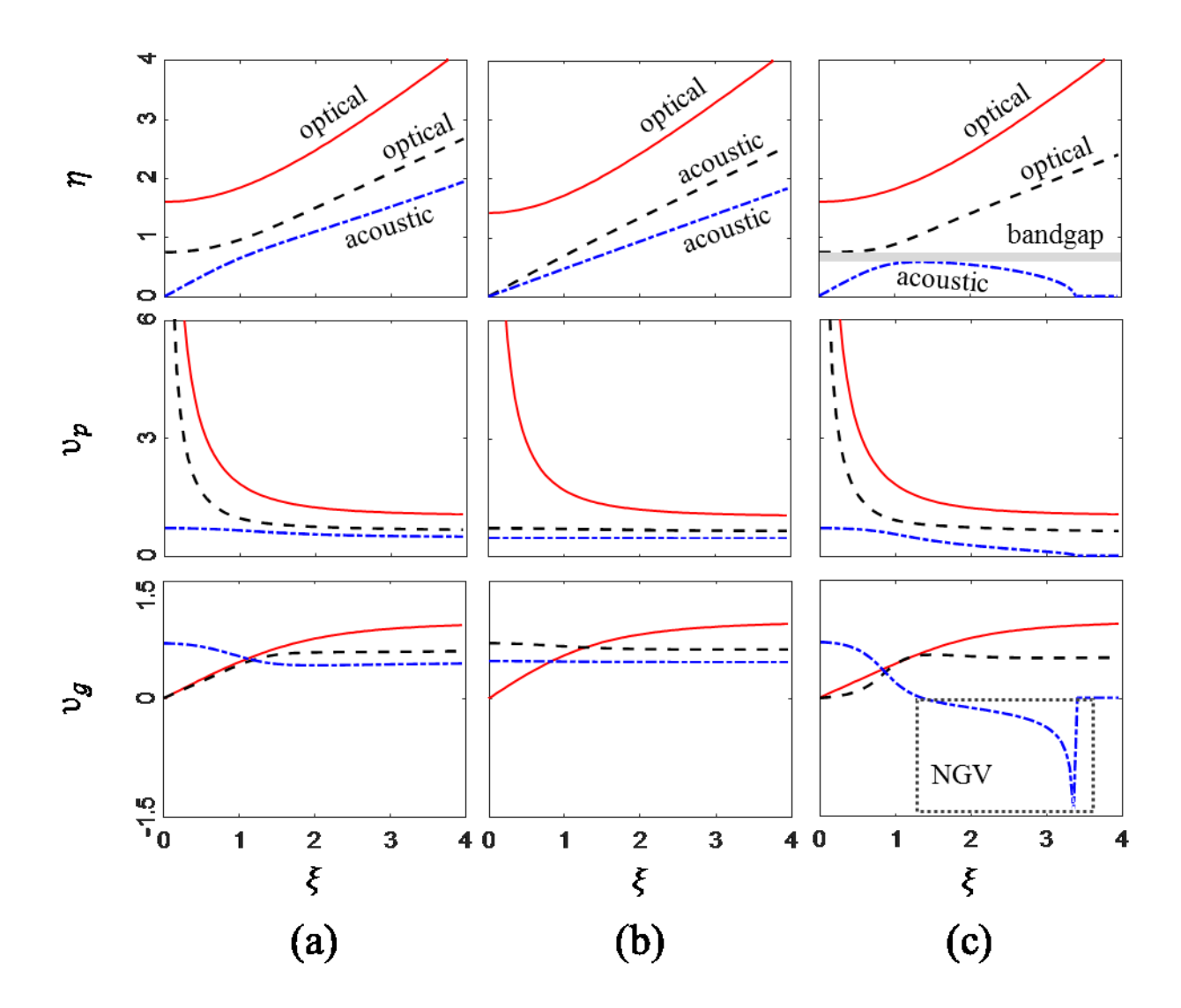
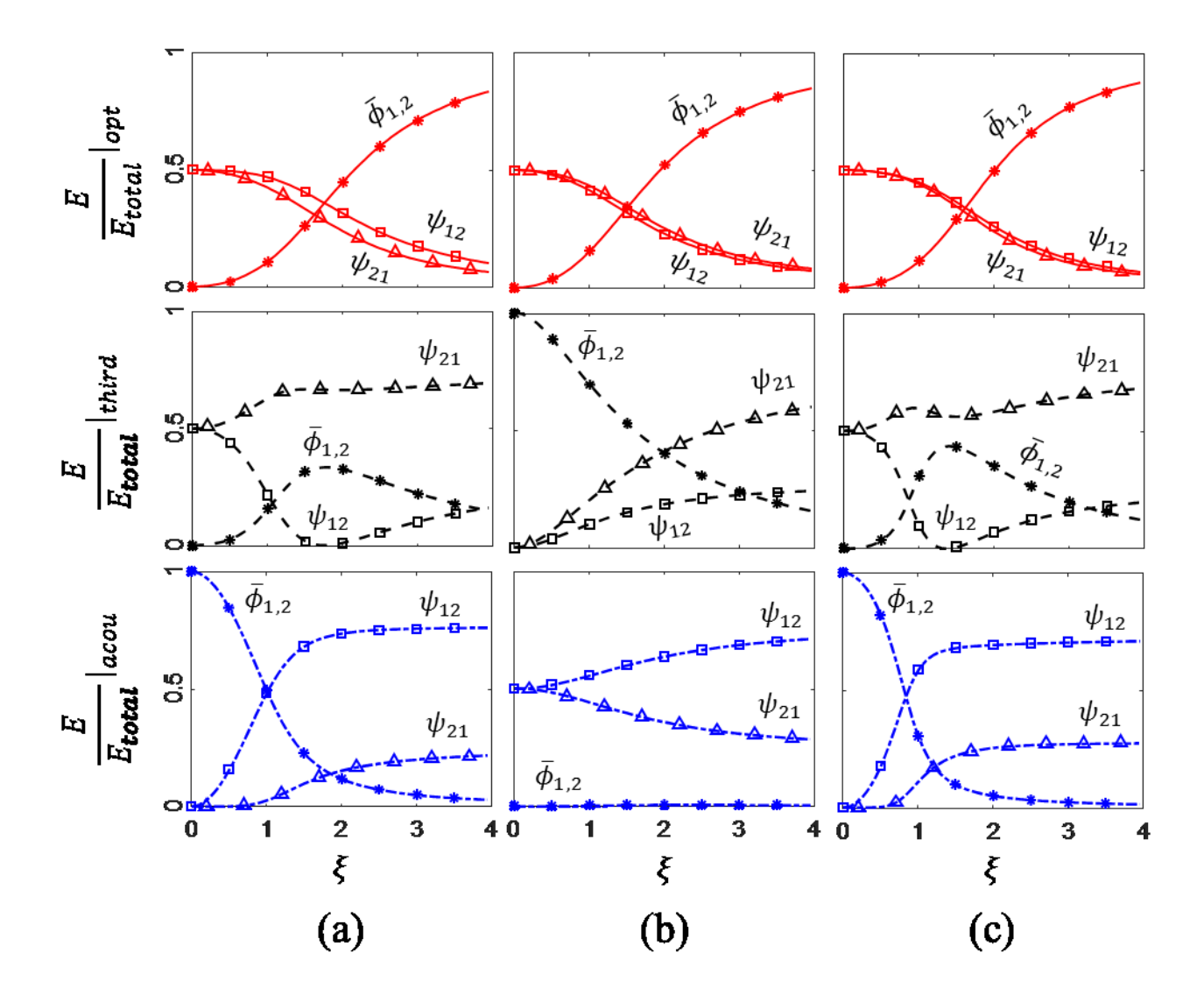


Fig. 7. Schematic of a 1D continuum in  $x_2$  direction with granular micro-structure in both  $x_1$ ' and  $x_2$ ' directions. A material point in the macro-scale coordinate system is itself a collection of grains that can differ in micro-density, micro-morphology and micro-mechanical properties.



**Fig. 8.** Dispersion curves, phase velocities  $\upsilon_p$ , and group velocities  $\upsilon_g$  for the optical branch, the third branch, and the acoustic branch, respectively, where solid line represents an optical branch, dash-dotted line represents an acoustic branch, and dashed line is either acoustic or optical (third branch). (a) A material with properties of  $\hat{\gamma}_A = 0.71$ ,  $\hat{\gamma}_1 = 0.5$ ,  $\hat{\gamma}_2 = 0.3$ ,  $\hat{\gamma}_4 = 0.1$ , and  $\chi = 0.8$ ; (b) A material with properties of  $\hat{\gamma}_A = 0.71$ ,  $\hat{\gamma}_1 = 0.5$ ,  $\hat{\gamma}_2 = 0.3$ ,  $\hat{\gamma}_4 = 0.1$ , and  $\chi = 1$ ; (c) A material with properties of  $\hat{\gamma}_A = 0.71$ ,  $\hat{\gamma}_1 = 0.2$ ,  $\hat{\gamma}_2 = 0.4$ ,  $\hat{\gamma}_4 = 0.1$ , and  $\chi = 0.8$ .



**Fig. 9.** Ratio of energy transferred by macro- and micro-scale degrees of freedom to the total energy for the optical branch, the third branch, and the acoustic branch, respectively, where solid line represents an optical branch, dash-dotted line represents an acoustic branch, and dashed line is either acoustic or optical (third branch). Lines with \*,  $\wedge$ , and  $\square$  represent energy transferred by macro-scale degree of freedom  $\bar{\phi}_1$ , and micro-scale degrees of freedom  $\psi_{21}$  and  $\psi_{12}$ , respectively. (a) A material with properties of  $\hat{\gamma}_A = 0.71$ ,  $\hat{\gamma}_1 = 0.5$ ,  $\hat{\gamma}_2 = 0.3$ ,  $\hat{\gamma}_4 = 0.1$ , and  $\chi = 0.8$ ; (b) A material with properties of  $\hat{\gamma}_A = 0.71$ ,  $\hat{\gamma}_1 = 0.5$ ,  $\hat{\gamma}_2 = 0.3$ ,  $\hat{\gamma}_4 = 0.1$ , and  $\chi = 1$ ; (c) A material with properties of  $\hat{\gamma}_A = 0.71$ ,  $\hat{\gamma}_1 = 0.2$ ,  $\hat{\gamma}_2 = 0.4$ ,  $\hat{\gamma}_4 = 0.1$ , and  $\chi = 0.8$ .

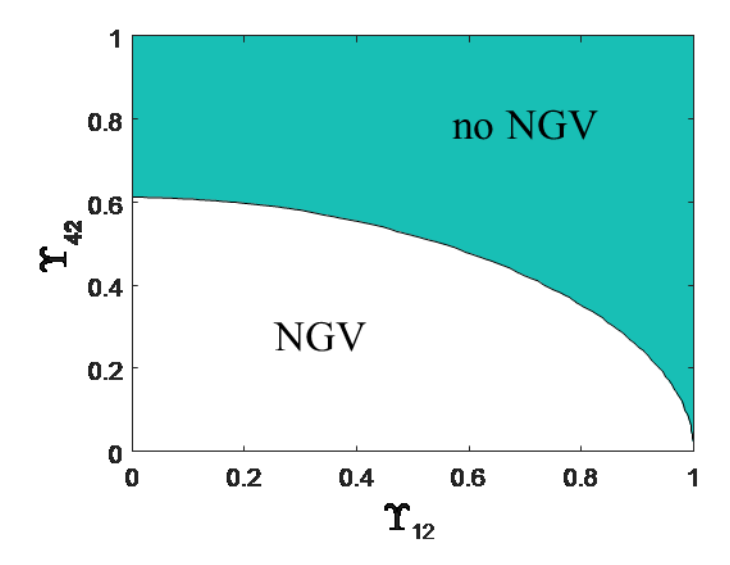


**Fig. 10.** White indicates the sets of parameters for which negative group velocity (NGV) occurs in the acoustic branch, while green color indicates the sets of parameters for which there is no NGV.